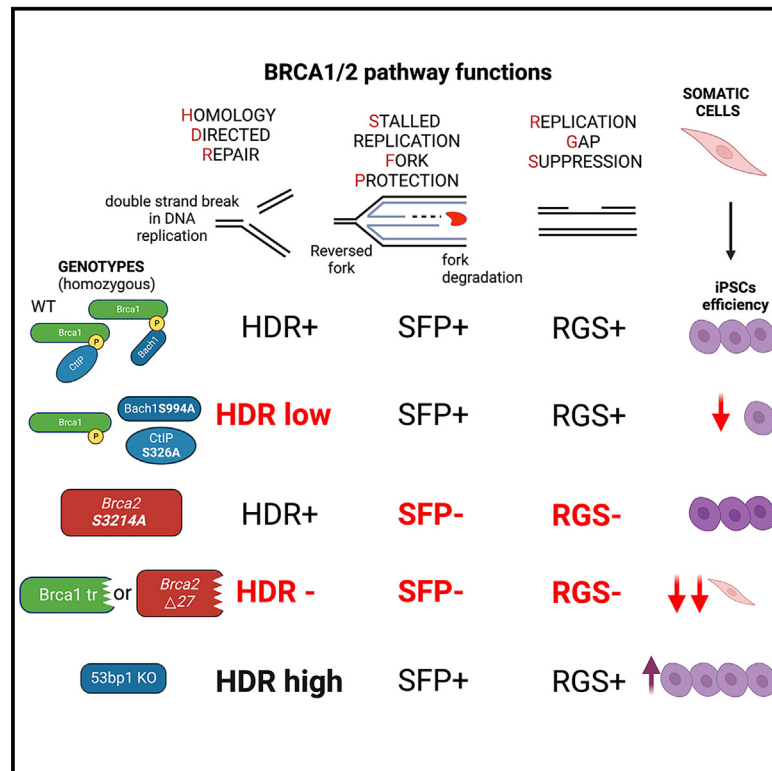


BRCA1 and 53BP1 regulate reprogramming efficiency by mediating DNA repair pathway choice at replication-associated double-strand breaks

Graphical abstract



Authors

Daniela Georgieva, Ning Wang, Angelo Tagliatela, ..., Alberto Ciccia, Richard Baer, Dieter Egli

Correspondence

de2220@cumc.columbia.edu

In brief

Using separation-of-function mutations in Brca1, Brca2, and interacting proteins, we show that homology-directed repair of replication-associated double-strand breaks is the critical function of the BRCA pathway in iPSC generation. Stalled replication fork protection and replication gap suppression are inconsequential to efficient iPSC induction.

Highlights

- Loss of 53BP1 increases HDR and reprogramming efficiency in mouse and human cells
- Brca1 phospho-interaction with Abraxas, Bach1, CtIP is required for HDR and reprogramming
- Stalled replication fork protection by Brca1 is dispensable for reprogramming
- Brca2 mutants with replication gap suppression deficiency reprogram efficiently



Article

BRCA1 and 53BP1 regulate reprogramming efficiency by mediating DNA repair pathway choice at replication-associated double-strand breaks

Daniela Georgieva,^{1,2,10} Ning Wang,^{1,2,10} Angelo Tagliatela,^{2,3} Stepan Jerabek,^{1,2,4} Colleen R. Reczek,^{6,9} Pei Xin Lim,⁵ Julie Sung,¹ Qian Du,¹ Michiko Horiguchi,^{6,8} Maria Jasin,⁵ Alberto Ciccia,^{2,3} Richard Baer,⁶ and Dieter Egli^{1,2,7,11,*}

¹Department of Pediatrics and Naomi Berrie Diabetes Center, Columbia University Irving Medical Center, New York, NY 10032, USA

²Columbia University Stem Cell Initiative, New York, NY 10032, USA

³Department of Genetics and Development, Herbert Irving Comprehensive Cancer Center, Columbia University Irving Medical Center, New York, NY 10032, USA

⁴Institute of Organic Chemistry and Biochemistry of the Czech Academy of Sciences, Flemingovo namesti 542/2, 160 00 Praha 6, Czech Republic

⁵Developmental Biology Program, Memorial Sloan Kettering Cancer Center, New York, NY 10065, USA

⁶Department of Pathology & Cell Biology, Institute for Cancer Genetics, Columbia University Irving Medical Center, New York, NY 10032, USA

⁷Department of Obstetrics and Gynecology, Columbia University Irving Medical Center, New York, NY 10032, USA

⁸Present address: Department of Pharmaceutics, Faculty of Pharmaceutical Sciences, Tokyo University of Science in Yamaguchi, Sanyo-Onoda City, Yamaguchi 7550015, Japan

⁹Present address: Department of Medicine, Northwestern University Feinberg School of Medicine, Chicago, IL 60611, USA

¹⁰These authors contributed equally

¹¹Lead contact

*Correspondence: de2220@cumc.columbia.edu

<https://doi.org/10.1016/j.celrep.2024.114006>

SUMMARY

Reprogramming to pluripotency is associated with DNA damage and requires the functions of the BRCA1 tumor suppressor. Here, we leverage separation-of-function mutations in BRCA1/2 as well as the physical and/or genetic interactions between BRCA1 and its associated repair proteins to ascertain the relevance of homology-directed repair (HDR), stalled fork protection (SFP), and replication gap suppression (RGS) in somatic cell reprogramming. Surprisingly, loss of SFP and RGS is inconsequential for the transition to pluripotency. In contrast, cells deficient in HDR, but proficient in SFP and RGS, reprogram with reduced efficiency. Conversely, the restoration of HDR function through inactivation of *53bp1* rescues reprogramming in *Brca1*-deficient cells, and *53bp1* loss leads to elevated HDR and enhanced reprogramming in mouse and human cells. These results demonstrate that somatic cell reprogramming is especially dependent on repair of replication-associated double-strand breaks (DSBs) by the HDR activity of BRCA1 and BRCA2 and can be improved in the absence of 53BP1.

INTRODUCTION

Somatic cells can be reprogrammed to pluripotency by ectopic expression of the four transcription factors OCT4, SOX2, KLF4, and cMYC (OSKM), which act as master regulators of the embryonic state.¹ The reprogrammed cell population, termed induced pluripotent stem cells (iPSCs), is endowed with the capacity to proliferate indefinitely and differentiate into any specialized cell type of the adult organism. These characteristics make iPSCs uniquely suitable for modeling human development and disease, drug discovery, and the design of patient-specific cell replacement therapies. Nonetheless, overexpression of the reprogramming factors OSKM or OSK (without cMYC) results in increased levels of DNA damage, marked by the formation of γ H2AX^{2,3} and FANCD2 nuclear foci.⁴ Importantly, increased γ H2AX and RPA foci are also seen during reprogramming by nuclear transfer, a

process that does not entail the overexpression of transcription factors,⁵ implying that DNA damage is intrinsic to cell reprogramming. Since DNA damage during reprogramming has the potential for adverse genetic consequences, which can compromise the utility of the resulting iPSCs, it is important to understand the origin and type of the damage as well as the mechanisms of repair.

Determining the genetic requirements for DNA repair factors during reprogramming can point to the type of DNA damage that arises during this process. Of note, somatic cell reprogramming is severely compromised by mutations or knockdown of proteins implicated in homology-directed repair (HDR) of DNA double-strand breaks (DSBs), including *Brca1* and *Brca2*,² CtIP,⁶ Rad51,² FancC and FancA,⁴ FancD2,⁷ and Atm.⁸ In contrast, ablation of the tumor suppressors *p53*,^{9,10} *p21*,¹¹ or *Rb*¹² results in more efficient iPSC generation, suggesting that



reprogramming is also governed by the molecular and cellular response to DNA damage.

Although BRCA1 has been implicated in many cellular processes, three aspects of its function are thought to be especially important for genome stability. First, BRCA1 is required for HDR, which repairs DSBs with high fidelity.¹³ BRCA1 promotes the HDR pathway at multiple stages, including an early commitment step in which the decision is made to repair a DSB either by HDR or by non-homologous end joining (NHEJ). BRCA1 favors the choice of HDR over NHEJ by facilitating DNA end resection, a process that converts DSB ends into 3' single-stranded DNA (ssDNA) overhangs, which serve as key intermediates for HDR.¹⁴ In addition, BRCA1 counters the activities of 53BP1, a protein that facilitates the recruitment of the shieldin complex to counteract DSB end resection and promote NHEJ.^{15,16} Second, BRCA1 protects stalled DNA replication forks from nucleolytic degradation.^{17,18} Interestingly, the HDR and stalled fork protection (SFP) activities of BRCA1 are genetically separable, and abrogation of SFP alone is sufficient to elicit chromosomal instability in response to replication stress.¹⁹ Likewise, several other HDR factors have been implicated in the stability of stalled replication forks. For example, Rad51 promotes remodeling of stalled replication forks²⁰ and CtIP protects stalled forks from nucleolytic degradation by DNA2.²¹ Of note, BRCA2, like BRCA1, also protects stalled forks from degradation by MRE11.^{17,22} Third, in addition to its involvement in HDR and SFP, BRCA1 has recently been shown to suppress the formation of ssDNA gaps arising during DNA replication in cancer cells,^{23,24} a function shared with BRCA2.^{25,26} Since HDR, SFP, and replication gap suppression (RGS) all contribute to the genome maintenance functions of BRCA1, each individual process may be critical for BRCA1-mediated somatic cell reprogramming.

RESULTS

Reprogramming and HDR are dependent on the interactions of BRCA1 with its BRCT phospho-ligands

Reprogramming is severely impaired in mouse fibroblasts that are homozygous for either of two pathogenic *Brca1* lesions (*Brca1^{tr}* and *Brca1^{S1598F}*).² The *Brca1^{tr}* allele encodes a C-terminally truncated protein that lacks several critical BRCA1 domains, including its serine/glutamine (SQ) cluster region, PALB2-binding sequence, and BRCT (BRCA1 C-terminal) motif²⁷ (Figure 1A). In contrast, the protein product of *Brca1^{S1598F}* harbors a single missense mutation that specifically disrupts the phosphate-binding cleft of the BRCT domain.²⁸ By virtue of its BRCT phospho-recognition domain, BRCA1 can interact with the phosphorylated isoforms of several DNA repair factors, including ABRAXAS, BACH1/BRIP1/FANCDJ, and CtIP.^{29–31} Since its interactions with each of these BRCT phospho-ligands are mutually exclusive, BRCA1 can form multiple distinct protein complexes *in vivo* (e.g., BRCA1 complexes A, B, and C) that may mediate different aspects of BRCA1 function.

To test whether the interaction of BRCA1 with one or more of its BRCT phospho-ligands is required for reprogramming, we examined mouse embryonic fibroblasts (MEFs) that are homozygous for serine-to-alanine substitutions in the critical phosphor-

ylation sites of Abraxas (S404A), Bach1 (S994A), and/or CtIP (S326A). Previous studies of *Brca1^{S1598F/S1598F}* cells have shown that BRCT phospho-recognition is required for both HDR²⁸ and SFP,¹⁹ as well as for reprogramming.² To ascertain whether these functions of *Brca1* are dependent on its interactions with Abraxas, Bach1, and/or CtIP, we bred mice harboring the different combinations of homozygous *Abraxas* (AA), *Bach1* (BB), and *CtIP* (CC) missense mutations and then evaluated HDR and SFP in MEFs and iPSC lines from these mice. Although double-mutant *AABB*, *BBCC*, and *AACC* embryos appeared to develop normally relative to their wild-type littermates, the triple *AABBCC* mutants were smaller on day E13.5 (Figure 1B). To assess HDR function in the different genotypes, we chose iPSCs as they can be grown in sufficient numbers for molecular analyses. Pluripotent stem cell lines were irradiated with 10 Gy ionizing irradiation (IR) and examined for the formation of irradiation-induced foci of the Rad51 recombinase by immunofluorescence microscopy at 1.5 h post treatment. Focus formation was significantly impaired in the triple-mutant *AABBCC* cells, while double-mutant *BBCC* and *AACC* showed modest, but not significant reduction (Figure 1C). To examine HDR competence, we conducted a CRISPR-Cas9-based DSB repair assay using cells that harbor a zsGreen-containing HDR template.³² A dramatic reduction in HDR activity was observed in triple-mutant *AABBCC* cells, while the double-mutant *BBCC* and *AACC* displayed a less severe, but significant HDR defect, as quantified using the dual-allele edited cells, which form a distinct, fluorescently brighter, population (Figure 1D). To measure SFP function, immortalized MEFs derived from E13.5 embryos were treated with HU, and the stability of stalled forks was assessed by analysis of 5-iodo-2'-deoxyuridine (IdU) and 5-chloro-2'-deoxyuridine (CldU)-stained DNA fibers, as previously described.¹⁹ The rationale for choosing immortalized MEFs was to allow for replicates, as triple-mutant embryos are rare, and primary MEFs were required for reprogramming studies. A marked reduction in the ratio of CldU/IdU track lengths, indicative of a profound SFP defect, was observed in triple-mutant *AABBCC* cells relative to wild-type controls (Figure 1E). In contrast, the track length ratios from each of the double mutants were indistinguishable from those of wild-type cells (Figure 1E). As such, the triple mutants, but not the double mutants, reproduce the HDR[−]SFP[−] phenotype observed in cells bearing tumor-associated *Brca1* mutations (*Brca1^{tr/tr}* or *Brca1^{S1598F/S1598F}* cells). Interestingly, *AACC* and *BBCC* double mutants were compromised for HDR, but retained normal SFP activity (Table S1), permitting further dissection of BRCA1 functions required for reprogramming.

During reprogramming, we observed a modest, but significant increase in γ H2AX focus formation in the triple *AABBCC* mutants; increases were also seen in double-mutant (*AABB*, *BBCC*, and *AACC*) MEFs, although not to significant levels (Figure 1F). While the yields of AP-positive colonies from double-mutant *BBCC* and *AACC* cells were lower than those of wild-type cells, the triple-mutant *AABBCC* displayed a marked reduction (~17-fold) in reprogramming efficiency, similar to the one reported for *Brca1^{tr/tr}* and *Brca1^{S1598F/S1598F}* MEFs (Figure 1G). Thus, the reductions in reprogramming efficiency (Figure 1G) paralleled those of HDR activity (Figure 1D), with modest decreases (~3-fold for HDR and 2- to 3-fold for reprogramming)

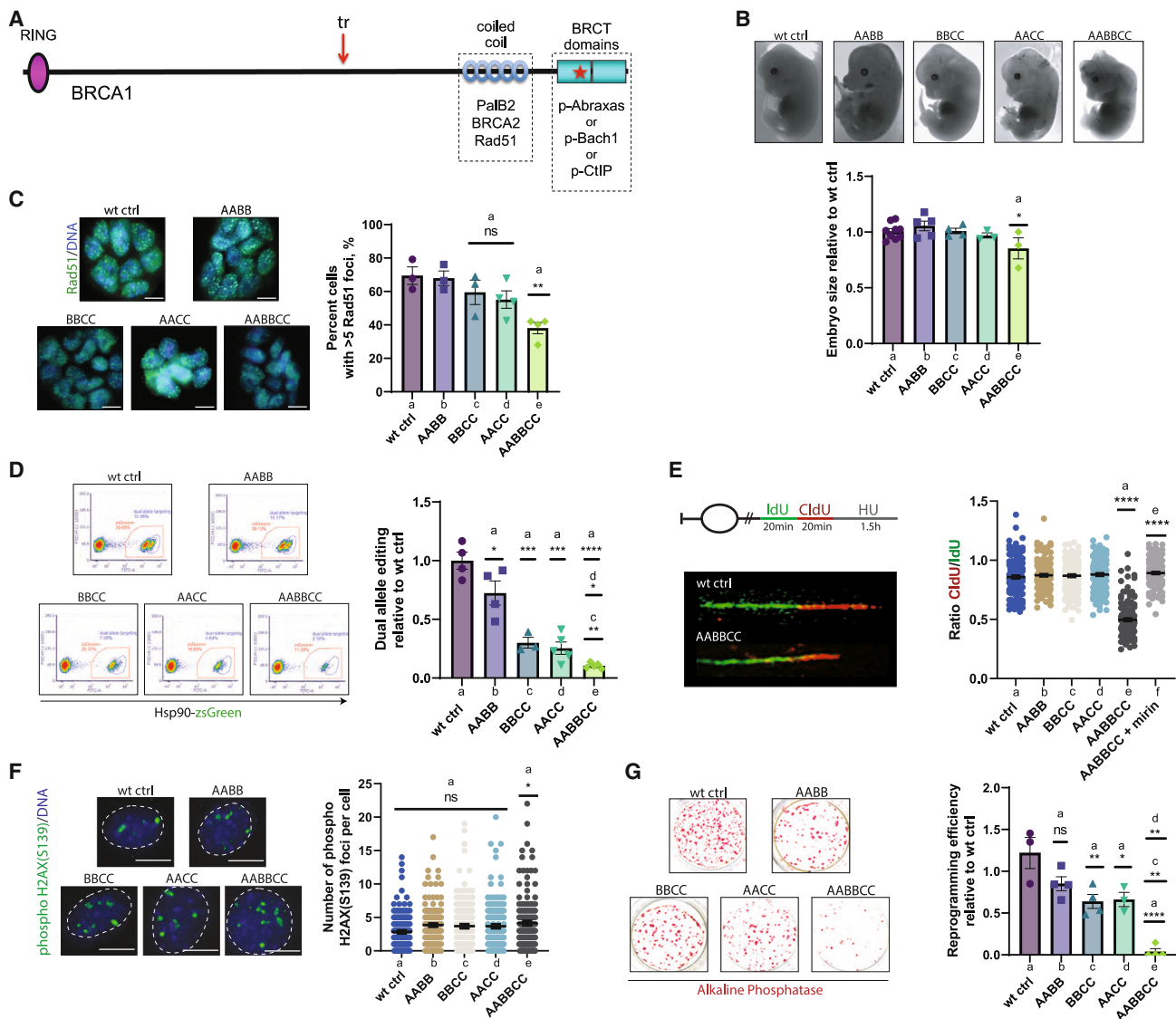


Figure 1. Phospho-protein interaction of Brca1 with Abraxas, Bach1, and CtIP is required for HDR and reprogramming

(A) Illustration of the BRCA1 polypeptide and simplified interaction engagements. The C-terminal BRCT domain of BRCA1 interacts in a mutually exclusive manner with the phosphorylated isoforms of ABRAXAS, BACH1, or CtIP to form distinct BRCA1 complexes. In addition, BRCA1 harbors a coiled-coil motif that mediates its interaction with PALB2 and the recruitment of BRCA2 and RAD51 to sites of DNA damage. The mutant mouse alleles used in this study include *Brca1^{tr}*, which encodes a pathogenic truncating mutation, denoted with a red arrow, that eliminates the BRCT domains, and *Abraxas^{S404A}*, *Bach1^{S994A}*, and *CtIP^{S326A}*, which each encode a missense mutation that eliminates a phosphorylation site necessary for the interaction of its protein product with the BRCT domain of BRCA1.

(B) Morphology and size of E13.5 embryos. The difference between wild-type (WT) ctrl and AABBC was evaluated with an unpaired two-tailed Student's t test; WT ctrl n = 9, AABB n = 5, BBCC n = 4, AACC n = 3, AABBC n = 3.

(C) Rad51 focus immunofluorescence and quantification in induced pluripotent stem cell (iPSC) lines treated with 10 Gy IR. Data were analyzed by one-way ANOVA; WT ctrl n = 3, AABB n = 3, BBCC n = 3, AACC n = 4, AABBC n = 4; A, *Abraxas^{S404A/S404A}*, B, *Bach1^{S994A/S994A}*, C, *CtIP^{S326A/S326A}*; scale bar: 10 μ m.

(D) CRISPR-Cas9-based HDR assay with iPSC lines, shown as a ratio of dual-allele targeting in each genotype vs. control. Statistical analysis by one-way ANOVA, except for BBCC vs. AABBC and AACC vs. AABBC, which used unpaired two-tailed Student's t tests; WT ctrl n = 4, AABB n = 4, BBCC n = 3, AACC n = 5, AABBC n = 5.

(E) DNA fork stalling in immortalized MEFs. At least 150 DNA fibers were measured per genotype. Analysis by one-way ANOVA.

(F) Immunofluorescence and quantification of phospho-H2AX(S139). Foci were counted on reprogramming day 5 in >138 cells/genotype. Statistical analysis by one-way ANOVA; scale bar: 5 μ m, applicable to all images.

(G) Alkaline phosphatase (AP) staining and reprogramming efficiency quantification. The number of AP-positive colonies is shown as a ratio to WT. Analysis by one-way ANOVA from biological replicates; WT ctrl n = 3, AABB n = 4, BBCC n = 4, AACC n = 3, AABBC n = 4.

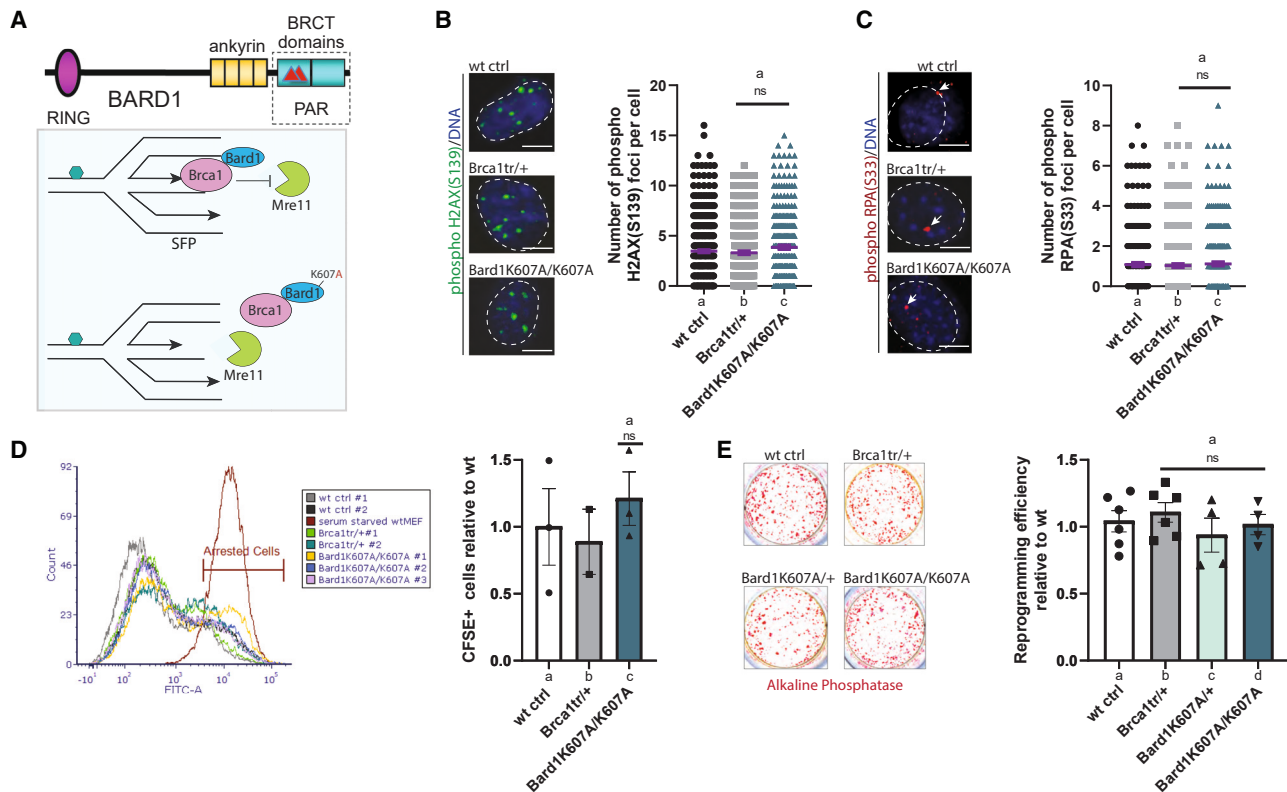


Figure 2. Stalled fork protection (SFP) is dispensable for reprogramming

(A) A schematic of Bard1-mediated SFP. The *Bard1*^{K607A} point mutation prevents the recruitment of the Brca1/Bard1 heterodimer to reversed stalled replication forks, which makes them vulnerable to Mre11-dependent degradation.

(B) Immunofluorescence and quantification of double-strand break (DSB) marker phospho-H2AX(S139). Foci were counted on reprogramming day 5 in ≥ 260 cells/genotype; statistical analysis by one-way ANOVA; scale bar: 5 μ m.

(C) Immunofluorescence and quantification of phospho-RPA(S33) on reprogramming day 5. Data were collected from ≥ 240 cells/genotype and analyzed by one-way ANOVA. The white arrows point to foci; scale bar: 5 μ m.

(D) Cell proliferation plots on reprogramming day 5. Arrested cells retain the dye CFSE and are detectable as a bright peak by flow cytometry. Analysis by one-way ANOVA; WT ctrl n = 3, *Brca1*^{tr/+} n = 2, *Bard1*^{K607A/K607A} n = 3.

(E) Alkaline phosphatase (AP) staining and reprogramming efficiency quantification. The number of AP-positive colonies is shown as a ratio to WT. Analysis by one-way ANOVA; WT ctrl n = 6, *Brca1*^{tr/+} n = 6, *Bard1*^{K607A/+} n = 4, *Bard1*^{K607A/K607A} n = 4; n represents biological replicates.

See also Figure S1.

in the *AACC* and *BBCC* mutants, which are SFP proficient, and a dramatic impairment (~ 10 -fold for HDR and >10 -fold for reprogramming) in *AABBCC* cells, which are both HDR and SFP deficient. We also noted a reduction in both HDR and reprogramming in the *AABB* genotype, although the differences were less than 2-fold. While the reductions in HDR and reprogramming within each mutant genotype were consistent, we recognized that they were not identical, perhaps reflecting threshold effects or the contribution of other repair mechanisms during reprogramming.

Loss of SFP does not affect reprogramming efficiency

The above experiments implicate HDR as a primary determinant of reprogramming efficiency but do not directly address the role of SFP. *In vivo*, BRCA1 exists as a heterodimer with BARD1, which also harbors a C-terminal BRCT domain.³³ The BRCT domain of BARD1 binds in a phospho-specific manner to poly(ADP-ribose) (PAR),³⁴ and this interaction is required for

recruitment of the BRCA1/BARD1 heterodimer to stalled replication forks and for BRCA1-mediated SFP activity¹⁹ (Figure 2A). Thus, by disrupting the interaction of Bard1 with PAR, *Bard1*^{K607A} and *Bard1*^{S563F} act as separation-of-function mutations that abrogate SFP without affecting HDR (Figures 2A and S1A); accordingly, *Bard1*^{K607A/K607A} and *Bard1*^{S563F/S563F} cells exhibit the HDR⁺SFP⁻ phenotype¹⁹ (Table S1). In addition, although HDR and most other biological functions of *BRCA1* are unaffected in heterozygotes, SFP is impaired in cells heterozygous for certain lesions in either *BRCA1*¹⁸ or *BARD1*,¹⁹ including *Bard1*^{K607A/+} and *Bard1*^{S563F/+} MEFs.

HDR-competent, SFP-deficient (i.e., HDR⁺SFP⁻) cells accumulate DNA breaks and chromosomal aberrations when exposed to replication stress.^{18,19,22} To assess the consequences of SFP deficiency on DNA damage during reprogramming, we quantified the appearance of γ H2AX and phospho-RPA(S33) foci on day 5 of reprogramming. This time point was chosen for analysis based on previous studies, which showed

elevated γ H2AX focus formation in *Brca1* mutant cells compared with controls from day 5 onward and persisting at least until day 16 of reprogramming.² The numbers of γ H2AX foci observed in *Brca1*^{tr/+} and *Bard1*^{K607A/K607A} cells were comparable to those of wild-type controls, indicating that SFP is not the primary mechanism preventing the accumulation of DNA damage during reprogramming (Figure 2B). The RPA/ssDNA filaments that form as a consequence of stalled fork processing are phosphorylated by the ATR kinase on Ser33 of the RPA2 polypeptide.^{35,36} *Brca1*^{tr/+} and *Bard1*^{K607A/K607A} mutants showed no increase in phospho(S33)-RPA2 foci relative to wild-type cells during reprogramming (Figure 2C). Proliferation rates of *Brca1*^{tr/+} and *Bard1*^{K607A/K607A} cells on day 5 of reprogramming were indistinguishable from those of wild-type controls (Figure 2D), while the size and morphology of *Brca1*^{tr/+} and *Bard1*^{K607A/K607A} embryos at day E13.5 were also normal (Figure S1B). Reprogramming efficiencies of all HDR⁺SFP⁻ genotypes tested (*Brca1*^{tr/+}, *Bard1*^{K607A/+}, *Bard1*^{K607A/K607A}, *Bard1*^{S563F/+}, and *Bard1*^{S563/S563F}), as measured by the formation of alkaline phosphatase (AP)-positive colonies, were indistinguishable from those of wild-type controls (Figures 2E and S1C). Thus, loss of *Brca1*-mediated SFP does not impair the efficiency of somatic cell reprogramming.

Restoring SFP in *Brca1*-mutant cells fails to improve reprogramming efficiency

The SNF2 family of DNA translocases SMARCAL1, ZRANB3, and HLTF remodels newly stalled replication forks into reversed (“chicken foot”) intermediate structures that can facilitate fork restart (Figure 3A).³⁷ Fork reversal generates a free DNA end, which, although relatively stable in normal cells, can serve as a substrate for Mre11-dependent degradation in *BRCA1*-mutant cells¹⁷; by blocking fork reversal, *Smarcal1* depletion can specifically rescue the SFP but not the HDR function of *BRCA1* mutant cells.³⁸ Thus, while *Brca1*^{tr/tr} cells display the HDR⁻SFP⁻ phenotype, *Brca1*^{tr/tr}*Smarcal1*^{-/-} cells are proficient in SFP and deficient in HDR (i.e., the HDR⁻SFP⁺ phenotype, Table S1).

To confirm that SFP is restored in *Brca1*^{tr/tr}*Smarcal1*^{-/-} cells during somatic cell reprogramming, we performed DNA fiber analysis after exposure to hydroxyurea (HU). In *Brca1*^{tr/tr}*Smarcal1*^{-/-} cells, the IdU/CldU ratios were restored to those of wild-type controls (Figure 3B). The SFP proficiency of *Brca1*^{tr/tr}*Smarcal1*^{-/-} cells was further established by DNA fiber analysis using the G-quadruplex stabilizing compound pyridostatin (PDS) (Figure S2A), which stalls replication forks in G-rich regions of the genome,³⁹ a physiologically relevant obstacle to DNA replication. As expected,³⁸ *Brca1*^{tr/tr}*Smarcal1*^{-/-} cells remained deficient for HDR (Figure 3C), confirming that they exhibit the HDR⁻SFP⁺ phenotype.

Consistent with studies of human breast epithelial cells,³⁸ DNA damage during reprogramming was significantly lower in *Brca1*^{tr/tr}*Smarcal1*^{-/-} cells relative to *Brca1*^{tr/tr} cells, as shown by reductions in both γ H2AX (Figure 3D) and phospho-RPA(S33) (Figure 3E) focus formation. Nonetheless, loss of *Smarcal1* (*Brca1*^{tr/tr}*Smarcal1*^{-/-} cells) failed to rescue either the proliferation defect (Figures 3F and S2B) or the elevated apoptosis (Figures 3G and S2C) of *Brca1*^{tr/tr} fibroblasts during reprogram-

ming. Moreover, *Brca1*^{tr/tr} and *Brca1*^{tr/tr}*Smarcal1*^{-/-} embryos were both significantly smaller on day E13.5 than either wild-type or *Smarcal1*^{-/-} embryos (Figure S2D). *Smarcal1*^{-/-} null and heterozygous *Smarcal1*^{-/+} MEFs reprogrammed with the efficiency of wild-type controls (Figures 3H, S2E, and S2F). In contrast, *Brca1*^{tr/tr}*Smarcal1*^{-/-} mutants, which have the HDR⁻SFP⁺ phenotype, displayed a severe defect in iPSC generation (>11-fold reduction), equivalent to that of HDR⁻SFP⁻ cells, such as *Brca1*^{tr/tr} and *AABBCC* (Figures 3H and 1G). Thus, restoration of SFP is insufficient to rescue the reprogramming deficiency of *BRCA1*-mutant cells. Even though the reprogramming efficiency in *Brca1*^{tr/tr} or *Brca1*^{tr/tr}*Smarcal1*^{-/-} and other HDR-deficient mutants such as *AABBCC* is severely reduced, once reprogrammed, iPSC lines could be established and propagated normally (Table S2). Thus, despite their HDR impairment, these genotypes proved permissive of the pluripotent stem cell fate.

Ablation of *53bp1* restores efficient reprogramming in *Brca1*-mutant cells

In normal cells, the decision to repair a DSB through either NHEJ or HDR is governed by the antagonistic relationship between 53BP1, which favors NHEJ by blocking resection of DSB ends, and the BRCA1/BARD1 heterodimer, which promotes HDR by displacing 53BP1^{14,16,40} (Figure 4A). Consequently, inactivation of *53bp1* can restore the HDR function of *Brca1*-mutant cells by allowing for resection and the subsequent formation of ssDNA filaments at DSB ends.^{15,41}

We examined whether restoring HDR in *Brca1*-mutant cells would also rescue their reprogramming potential. Consistent with published literature, we confirmed that *Brca1*^{tr/tr}*53bp1*^{-/-}, but not *Brca1*^{tr/tr}, iPSCs are competent for HDR (Figure 4B). Previous studies have shown that the impact of 53BP1 loss on SFP varies between cell types⁴²; here, we observed that the SFP defect of *Brca1*^{tr/tr} cells was partially restored on a *53bp1*-null background in *Brca1*^{tr/tr}*53bp1*^{-/-} MEFs (Figure 4C). Moreover, loss of *53bp1* in *Brca1*^{tr/tr}*53bp1*^{-/-} cells reduced γ H2AX and phospho-RPA(S33) focus formation relative to *Brca1*^{tr/tr} (Figures 4D and 4E) while also restoring proliferation (Figures 4F and S3A) and reducing the levels of apoptosis during reprogramming (Figures 4G and S3B). Importantly, the severe reprogramming defect of *Brca1*^{tr/tr} MEFs was fully rescued by loss of *53bp1*, as shown by the restoration in AP⁺ colony numbers in *Brca1*^{tr/tr}*53bp1*^{-/-} cells (Figures 4H, S3C, and S3D). This rescue was also reflected in the increased numbers of Nanog-positive colonies (Figure 4I) and of Nanog-positive cells (Figures S3E and S3F). Concordance between AP and Nanog staining in the quantification of reprogramming efficiency was also confirmed in an earlier report.² Collectively, these findings indicate that efficient HDR promotes somatic cell reprogramming.

Loss of *53bp1* increases HDR activity and reprogramming efficiency in *Brca1*-proficient cells

53BP1 regulates the balance between DSB repair pathways by promoting NHEJ at the expense of HDR.^{15,16,40,41} Accordingly, we observed that the HDR capacity of *53bp1*^{-/-} cells is modestly (1.2-fold), but significantly elevated relative to that of the wild-type controls (Figure 4B). Of note, the levels of

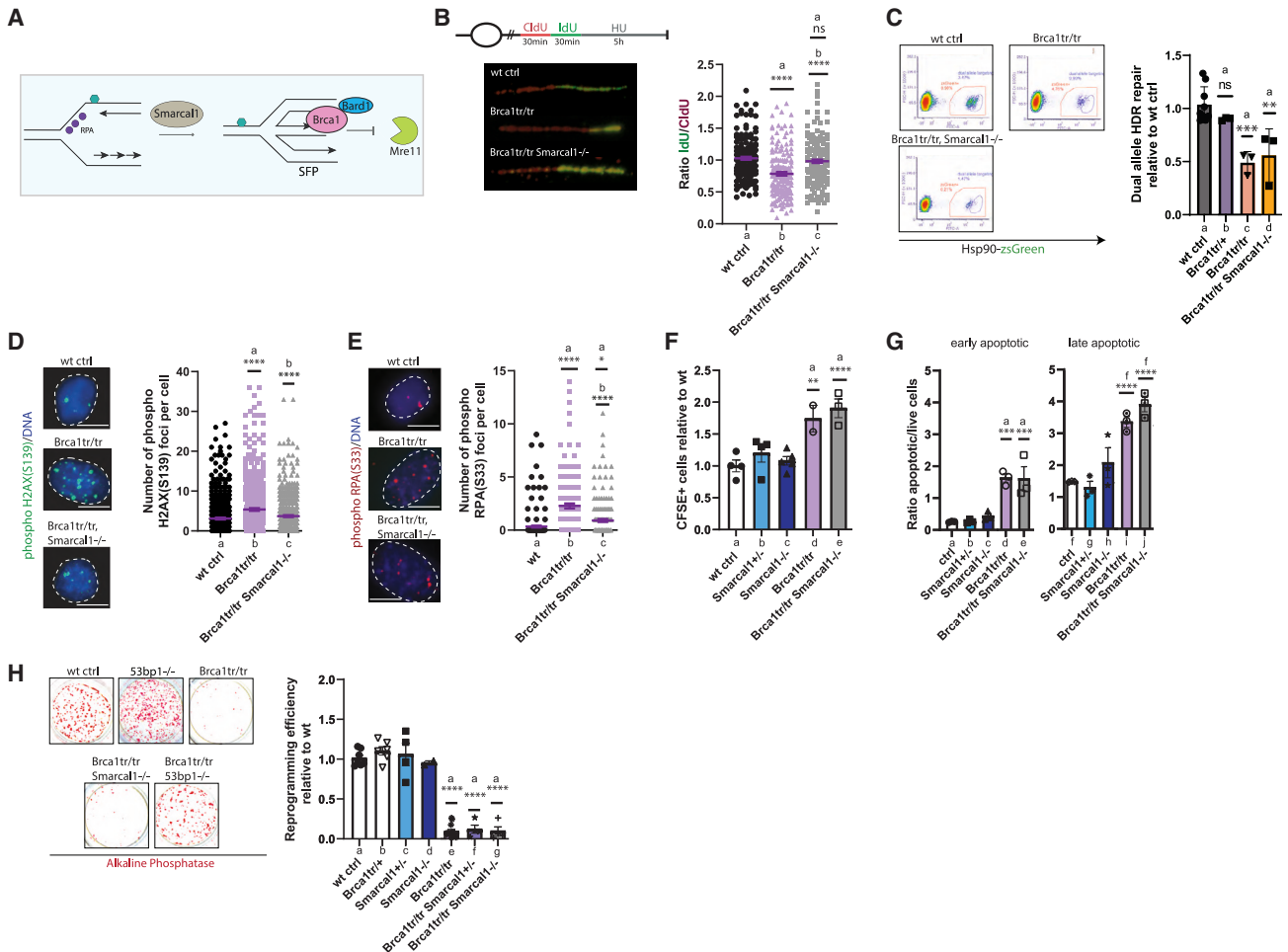


Figure 3. SFP-specific rescue of *Brca1* function fails to restore reprogramming

(A) A schematic for rescuing SFP in *Brca1*-mutant cells by ablation of *Smarcal1*.

(B) DNA fiber analysis in a fork stalling assay with hydroxyurea (HU) on reprogramming day 5. At least 120 DNA fibers were measured per genotype. Analysis by one-way ANOVA.

(C) CRISPR-Cas9-based HDR assay with induced pluripotent stem cell (iPSC) lines. Data are shown as a ratio of dual-allele targeting in each genotype relative to control. Statistical analysis by one-way ANOVA; WT ctrl n = 9, *Brca1*^{tr/+} n = 3, *Brca1*^{tr/tr} n = 3, *Brca1*^{tr/tr} *Smarcal1*^{-/-} n = 3.

(D) Immunofluorescence and quantification of the double-strand break (DSB) marker phospho-H2AX(S139). Foci were counted on reprogramming day 5 (≥ 410 cells/genotype) and statistical analysis was performed with one-way ANOVA. Scale bar: 5 μ m.

(E) Immunofluorescence and quantification of ssDNA marker phospho-RPA(S33) on reprogramming day 5. Data were collected from ≥ 140 cells per genotype and analyzed by one-way ANOVA. Scale bar: 5 μ m.

(F) Cell proliferation analysis with CFSE on reprogramming day 5. Statistical analysis by one-way ANOVA; WT ctrl n = 4, *Smarcal1*^{+/-} n = 4, *Smarcal1*^{-/-} n = 5, *Brca1*^{tr/tr} n = 2, *Brca1*^{tr/tr} *Smarcal1*^{-/-} n = 3.

(G) Apoptosis analysis with Annexin V and propidium iodide (PI) on reprogramming day 5. Analysis by one-way ANOVA; WT ctrl n = 3, *Smarcal1*^{+/-} n = 3, *Smarcal1*^{-/-} n = 3, *Brca1*^{tr/tr} n = 3, *Brca1*^{tr/tr} *Smarcal1*^{-/-} n = 3.

(H) Alkaline phosphatase (AP) staining and reprogramming efficiency quantification. The number of AP-positive colonies is shown as a ratio to wild type. Data analysis by one-way ANOVA; WT ctrl n = 7, *Brca1*^{tr/+} n = 6, *Smarcal1*^{+/-} n = 4, *Smarcal1*^{-/-} n = 2, *Brca1*^{tr/tr} n = 12, *Brca1*^{tr/tr} *Smarcal1*^{+/-} n = 4, *Brca1*^{tr/tr} *Smarcal1*^{-/-} n = 4; n represents biological replicates.

See also Figure S2.

proliferation (Figures 4F and S3A) and apoptosis (Figure 4G) were indistinguishable between *53bp1*^{-/-} and wild-type cells and no size differences were observed in *53bp1*^{-/-} embryos compared to wild-type controls at day E13.5 of development (Figure S3G).

Loss of *53bp1* was associated with a modest (up to 1.4-fold), but significant increase in reprogramming efficiency as

measured by AP⁺ colony numbers relative to both wild-type cells (Figure 4H) and SFP-deficient, but HDR-competent, *Brca1*^{tr/+} mutants (Figures 4H and S3D). The enhanced reprogramming potential of the *53bp1*^{-/-} genotype relative to wild type was further corroborated by immunofluorescence and flow cytometry data, which showed a 2-fold increase in the number of cells expressing the pluripotency maker Nanog (Figures 4I, S3E, and

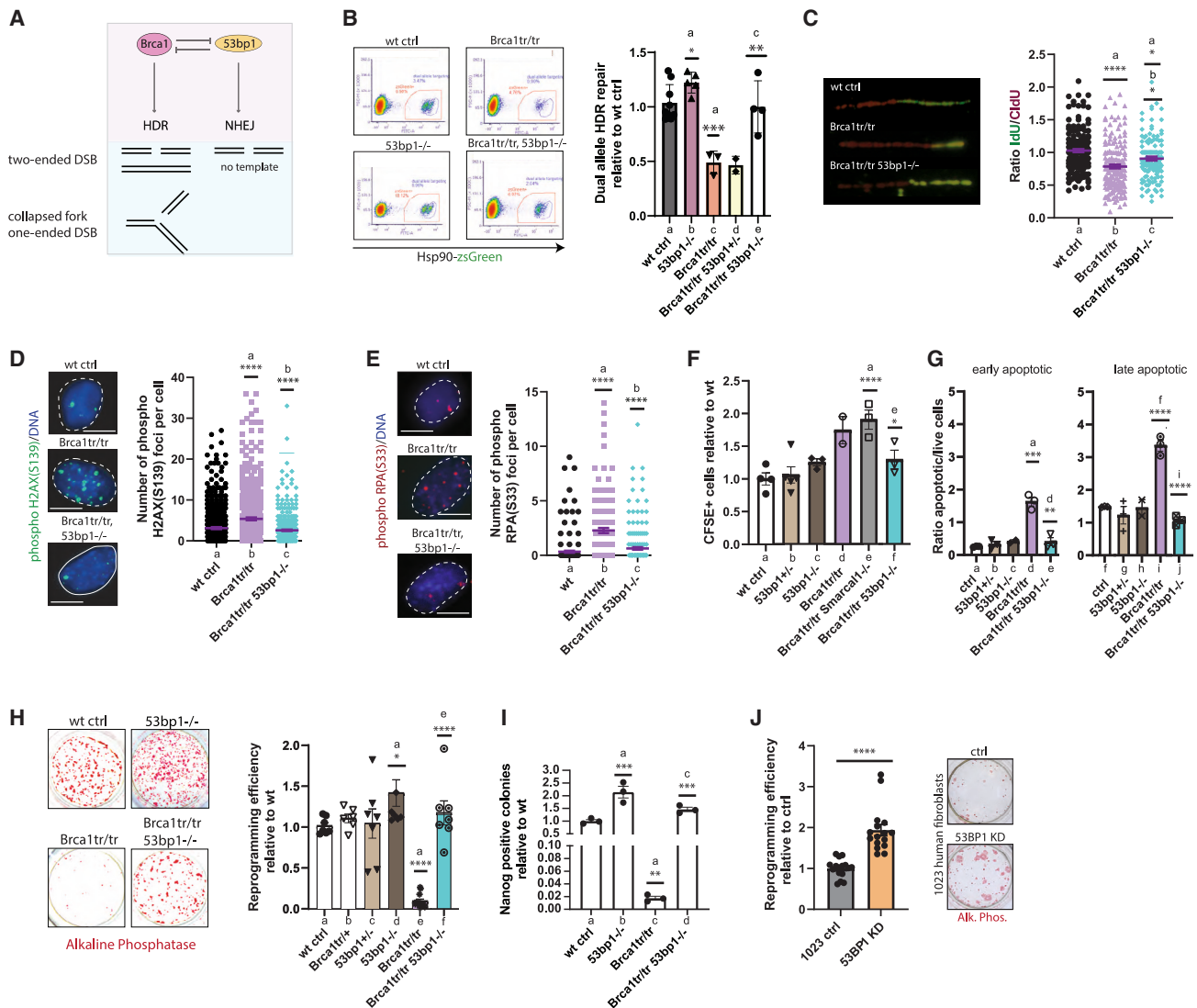


Figure 4. HDR-specific rescue of *Brca1* function restores reprogramming

(A) A schematic for rescuing HDR in *Brca1*-mutant cells by ablation of *53bp1*. Relevant substrates that can be repaired by HDR or NHEJ are shown.

(B) CRISPR-Cas9-based HDR assay with induced pluripotent stem cell (iPSC) lines. Data are shown as a ratio of dual-allele targeting in each genotype to dual-allele targeting in the control. Statistical analysis using one-way ANOVA, except for the comparison between WT ctrl and *53bp1*^{-/-}, evaluated with a two-tailed, unpaired Student's t test; WT ctrl n = 9, *53bp1*^{-/-} n = 5, *Brca1*^{tr/tr} n = 3, *Brca1*^{tr/tr}*53bp1*^{+/-} n = 2, *Brca1*^{tr/tr}*53bp1*^{-/-} n = 4.

(C) DNA fiber analysis in a fork stalling assay with hydroxyurea (HU) on reprogramming day 5. At least 120 DNA fibers were measured per genotype, and the data were analyzed by one-way ANOVA.

(D) Immunofluorescence and quantification of phospho-H2AX(S139). Foci were counted on reprogramming day 5 (≥410 cells/genotype) and statistical analysis was performed with one-way ANOVA.

(E) Immunofluorescence and quantification of ssDNA marker phospho-RPA(S33) on reprogramming day 5 (≥140 cells per genotype), analyzed by one-way ANOVA. For control and *Brca1* mutants, images are identical for (D) and (E) here and in Figures 3D and 3E, respectively.

(F) Cell proliferation analysis with CFSE dye on reprogramming day 5. Statistical analysis by one-way ANOVA; WT ctrl n = 4, *53bp1*^{+/-} n = 5, *53bp1*^{-/-} n = 3, *Brca1*^{tr/tr} n = 2, *Brca1*^{tr/tr}*Smarca1*^{-/-} n = 3, *Brca1*^{tr/tr}*53bp1*^{-/-} n = 3.

(G) Apoptosis analysis with Annexin V and propidium iodide (PI) on reprogramming day 5, analyzed by one-way ANOVA; WT ctrl n = 3, *53bp1*^{+/-} n = 3, *53bp1*^{-/-} n = 2, *Brca1*^{tr/tr} n = 3, *Brca1*^{tr/tr}*53bp1*^{-/-} n = 3.

(H) Alkaline phosphatase (AP) staining and reprogramming efficiency quantification. Number of AP-positive colonies is shown as a ratio to WT and analyzed by one-way ANOVA; WT ctrl n = 7, *Brca1*^{tr/+} n = 6, *53bp1*^{+/-} n = 7, *53bp1*^{-/-} n = 8, *Brca1*^{tr/tr} n = 12, *Brca1*^{tr/tr}*53bp1*^{-/-} n = 7.

(I) Quantification of Nanog-positive colonies in the indicated genotypes, analyzed with one-way ANOVA; n = 3 for each genotype.

(J) AP staining and reprogramming efficiency quantification in human 1023 fibroblasts from adult skin biopsy in control and 53BP1 knockdown (KD) conditions. Cells were fixed on day 25 post reprogramming factor transduction and the statistical analysis used an unpaired, two-tailed Student's t test; ctrl n = 16, 53BP1 KD n = 16. Samples with n = 2 were not used for statistical comparisons. All numbers indicated are biological replicates. Error bars represent the standard error of the mean. See also Figure S3.

S3F). Increased reprogramming efficiency was also demonstrated in human dermal fibroblasts. Downregulation of 53BP1 by RNAi during reprogramming (Figures S3I and S3J) led to an ~2-fold increase in AP⁺ iPSC colony formation (Figures 4J, S3J, and S3K).

To investigate how 53BP1 affects iPSC generation, we examined 53bp1 focus formation in response to DNA damage during reprogramming. As expected, *Brca1*^{tr/tr} cells, which are defective for both HDR and SFP, displayed increased levels of 53bp1 foci relative to wild-type cells (Figure 5A). In contrast, all HDR⁺ SFP⁻ cells, including *Brca1*^{tr/+}, *Bard1*^{K607A/K607A}, and *Bard1*^{S563F/S563F} cells, formed 53bp1 foci in numbers similar to those observed in the wild-type cells (Figure 5A). Notably, 53bp1 focus formation in *Brca1*^{tr/tr}*Smarcal1*^{-/-} cells, which display the HDR⁻SFP⁺ phenotype, occurred at elevated levels, similar to those of *Brca1*^{tr/tr} cells, despite restoration of SFP activity (Figure 5A). These results reveal a negative correlation between iPSC generation and 53bp1 assembly at sites of DSB repair.

In addition to its role in DSB repair by NHEJ, 53BP1 has a separate function in the stimulation of p53-dependent transcription of the cell cycle inhibitor p21 in human metastatic adenocarcinoma.⁴³ Another study showed normal stabilization of p53 and IR-induced upregulation of p21 in *53bp1*^{-/-} mouse thymocytes,⁴⁴ demonstrating that the impact of 53bp1 on p53 function may vary with cell type. Nonetheless, since downregulation of either p53 or p21 has been shown to improve iPSC generation,¹¹ we examined the expression of p21 during reprogramming. We detected no changes in proliferation (Figures 4F and S3A) or apoptosis (Figure 4G) of *53bp1*^{-/-} cells relative to wild-type controls and no difference in p21 expression levels in primary MEFs (Figures S3L and S3M) or during reprogramming (Figure 5B). Therefore, the enhanced reprogramming efficiency of *53bp1*^{-/-} cells is not due to compromised expression of the p53 transcriptional target p21.

Replication-associated DSBs limit somatic cell reprogramming

The genetic requirements for DSB repair during iPSC generation point to the type of DNA damage that impairs reprogramming. DSBs arising during replication at stalled and collapsed forks are typically one-ended,^{45–47} and in normal cells, these breaks are preferentially repaired by HDR.^{40,48} In contrast, two-ended DSBs can be induced by exogenous sources, such as IR or Cas9 cleavage, or occur endogenously due to oxidative stress or the genetic rearrangements during normal lymphocyte development. While two-ended DSBs are productively repaired by either NHEJ or HDR, one-ended DSBs from replication intermediates are not suitable for NHEJ, and their misrepair can yield aberrant chromosomal rearrangements.

To determine which types of DSBs affect the efficiency of iPSC generation, we treated reprogramming MEFs with the DNA polymerase inhibitor aphidicolin, which can induce replication-associated DSBs due to replication fork slowing.⁴⁸ Treatment of uninfected wild-type fibroblasts with a low concentration of aphidicolin resulted in elevated numbers of 53bp1 nuclear foci (Figure 5C). Wild-type cells exposed to low aphidicolin throughout an 8 day period during reprogramming showed a

2-fold reduction in iPSC colony formation (Figure 5D). The inhibitory effect of aphidicolin on reprogramming was more pronounced in *Brca1*^{tr/tr} cells (Figure 5E). (A higher bar in Figures 5E–5H corresponds to greater sensitivity and lower reprogramming efficiency relative to untreated cells.) *53bp1*^{-/-} mutant MEFs were less sensitive to aphidicolin than wild-type cells, and *Brca1*^{tr/tr}*53bp1*^{-/-} cells were less sensitive to aphidicolin than *Brca1*^{tr/tr} cells (Figure 5E). Since low concentrations of aphidicolin increase chromosome breakage,⁴⁹ these results suggest that efficient reprogramming is dependent on the efficient repair of replication-induced lesions by HDR.

To further explore the impact of replication-associated DSBs on cell reprogramming, we also tested topotecan, a topoisomerase I inhibitor. At low concentrations, topotecan generates single-strand nicks that can be converted to one-ended DSBs during DNA replication.⁴⁷ While topotecan treatment slightly reduced the reprogramming efficiency of wild-type cells (Figure 5F), it had a pronounced negative effect on iPSC generation from HDR-deficient *Brca1*^{tr/tr} MEFs (Figure 5F). This phenotype was partially rescued in HDR-proficient *Brca1*^{tr/tr}*53bp1*^{-/-} cells (Figure 5F). Furthermore, loss of 53bp1 in wild-type MEFs also decreased their sensitivity to topotecan exposure during reprogramming (Figure 5F). These results indicate that the HDR-mediated repair of replication-associated DSBs is a limiting factor for efficient iPSC generation.

It was previously reported that Parp1 is required for OSKM-mediated reprogramming in MEFs⁵⁰ and that Parp1 inhibition results in the accumulation of replication-associated DSBs.^{51,52} To determine the consequences of Parp1 inhibition on reprogramming, we exposed different genotypes to olaparib. Although a low concentration of olaparib (50 nM) did not affect the reprogramming efficiency of wild-type controls (Figures 5G and S4C), it reduced the reprogramming capacity of HDR-deficient *Brca1*-mutant MEFs (Figure 5G). As with aphidicolin and topotecan, the impaired reprogramming of *Brca1*-mutant cells was fully restored on a *53bp1*-null background (Figure 5G). Although this result is consistent with the genetic requirements for the repair of replication-associated DSBs, it should be noted that PARP inhibition also increases the incidence of ssDNA gaps.^{53,54} Since BRCA1-deficient cells have elevated frequencies of ssDNA gaps both under unstressed conditions and upon exposure to DNA-damaging agents,^{23,24} the impact of ssDNA gap formation on reprogramming is addressed in the following Figure 6 and associated chapter.

To evaluate the impact of two-ended DSBs on iPSC formation, we administered a single dose (1, 3, or 6 Gy) of IR 1 day after doxycycline induction of the OSKM reprogramming factors. Although IR treatment reduced reprogramming efficiency in all genotypes tested, *53bp1*^{-/-} cells were modestly, but significantly more sensitive than wild-type cells at all levels of IR exposure (Figures 5H, S4A, and S4B). This result contrasts with the lower sensitivity of *53bp1*^{-/-} fibroblasts to treatment with aphidicolin (Figure 5F) or topotecan (Figure 5F) during reprogramming. In *Brca1*^{tr/tr} cells, IR at all doses elicited a marked reduction in reprogramming efficiency (Figures 5H, S4A, and S4B). However, in contrast to aphidicolin or topotecan exposure, the reprogramming efficiency of IR-treated *Brca1*^{tr/tr} MEFs was only partially restored by loss of 53bp1 in *Brca1*^{tr/tr} cells

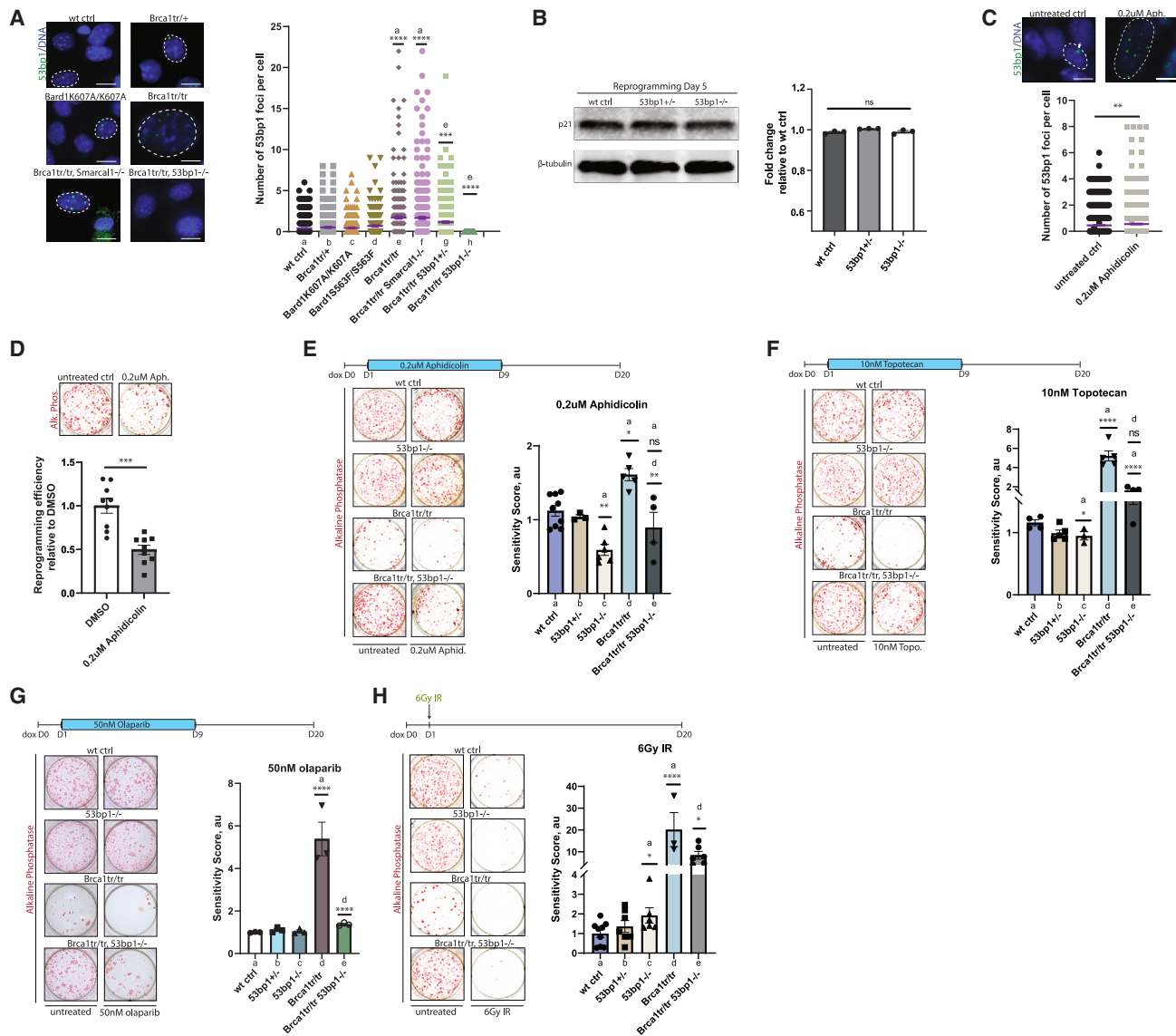


Figure 5. Replication-induced DNA double-strand breaks limit reprogramming

(A) Immunofluorescence of 53bp1 foci on reprogramming day 5. Data from at least 280 cells/genotype were analyzed by one-way ANOVA; scale bar: 10 μm. (B) Western blot and signal quantification of p21 from cells of the indicated genotypes on reprogramming day 5. Analysis by one-way ANOVA; n = 3 for each genotype. (C) Staining and quantification of 53bp1 foci in wild-type uninfected primary MEFs, treated with 0.2 μM aphidicolin for 3 days. At least 1,000 cells were analyzed per condition; statistical analysis used an unpaired two-tailed Student's t test; scale bar: 10 μm. (D) Alkaline phosphatase (AP) staining of control and 0.2 μM aphidicolin-treated wild-type cells for 8 days during reprogramming. Analysis was performed with an unpaired, two-tailed Student's t test. n = 9 untreated, n = 9 aphidicolin treated. (E–G) A higher column shows a greater sensitivity of the genotype to the drug applied. (E) Alkaline phosphatase (AP) staining and genotype-specific sensitivity evaluation to treatment with 0.2 μM aphidicolin for 8 days during reprogramming. Analysis by one-way ANOVA; WT ctrl n = 9, *53bp1*^{+/-} n = 3, *53bp1*^{-/-} n = 6, *Brca1*^{tr/tr} n = 5, *Brca1*^{tr/tr} *53bp1*^{-/-} n = 4. (F) AP staining and genotype-specific sensitivity to treatment with 10 nM topotecan for 8 days during reprogramming. Analysis by one-way ANOVA. The comparison between WT ctrl and *53bp1*^{-/-} was carried out with an unpaired two-tailed Student's t test; WT ctrl n = 4, *53bp1*^{+/-} n = 5, *53bp1*^{-/-} n = 3, *Brca1*^{tr/tr} n = 5, *Brca1*^{tr/tr} *53bp1*^{-/-} n = 4. (G) AP staining and genotype-specific sensitivity to treatment with 50 nM olaparib for 8 days during reprogramming. Analysis by one-way ANOVA; n = 3 for each genotype. (H) AP staining and genotype-specific sensitivity to treatment with a single dose of 6 Gy IR 1 day post reprogramming factor induction. Analysis by one-way ANOVA. The comparison between WT ctrl and *53bp1*^{-/-} was carried out with an unpaired two-tailed Student's t test on biological replicates; WT ctrl n = 9, *53bp1*^{+/-} n = 7, *53bp1*^{-/-} n = 6, *Brca1*^{tr/tr} n = 3, *Brca1*^{tr/tr} *53bp1*^{-/-} n = 6.

See also Figure S4.

(*Brca1^{tr/tr}* vs. *Brca1^{tr/tr}53bp1^{-/-}* genotypes) (Figures 5H, S4A, and S4B). These results indicate that increasing the load of two-ended DSBs during reprogramming impedes iPSC generation in 53bp1-null cells, presumably reflecting the role of 53bp1 in NHEJ repair of two-ended DSBs.⁵⁵ Collectively, the genetic requirements for the repair of replication-associated DSBs match the genetic requirements for efficient reprogramming, while repair of two-ended DSBs does not.

HDR of DSBs, rather than ssDNA gap suppression, is the primary function of BRCA1 in reprogramming

To determine the role RGS in somatic cell reprogramming, we examined ssDNA gap formation using the S1 nuclease assay. The S1 nuclease specifically cleaves ssDNA and thereby shortens IdU/CldU-labeled replication tracks with ssDNA gaps⁵⁶ (Figure 6A). Cells homozygous for *Brca1^{tr/tr}* displayed a significant increase in ssDNA gap formation both in reprogrammed iPSC lines (Figure 6B) and in MEFs undergoing reprogramming (Figures S4D and S4E).

To ascertain whether reprogramming is dependent on HDR, RGS, or both, we examined ssDNA gap formation in the AABCC genotype, which displays a profound defect in reprogramming efficiency (Figure 1G), comparable to the pathogenic *Brca1* mutants *Brca1^{tr/tr}* and *Brca1^{S1598F/S1598F}*.² Contrasting the increased ssDNA gap formation observed in *Brca1^{tr/tr}* and *Brca1^{S1598F/S1598F}* MEFs, ssDNA gaps were not elevated in AABCC cells relative to wild-type controls (Figures 6C, S4D, and S4E). Likewise, ssDNA gaps were not detected in the double-combination mutants AACC and BBCC (Figures 6C, S4D, and S4E), which displayed modest, but significant reductions in both HDR (Figure 1D) and reprogramming potential (Figure 1G). In our experiments, the difference in spontaneous ssDNA gap formation between the *Brca1^{tr/tr}* and the AABCC genotypes implies that deficiency in HDR, and not RGS, is primarily responsible for the impaired reprogramming capacity of *Brca1*-mutant cells.

To further examine the role of RGS, we also evaluated the impact of two previously characterized *Brca2* mutations on iPSC formation: *Brca2^{S3214A}* (referred to as *Brca2^{SA}*), which encodes a serine-to-alanine substitution of amino acid 3,214, and *Brca2^{Δ27}*, which gives rise to a C-terminally truncated *Brca2* polypeptide lacking residues 3,140–3,328, including S3,214. Heterozygous and homozygous *Brca2^{SA}* mutants are both deficient for RGS and SFP but retain HDR function.⁵⁷ As shown in Figure 6D, RGS in *Brca2^{SA/SA}* cells is also impaired during reprogramming. Despite RGS deficiency, however, the reprogramming capacity of *Brca2^{SA/SA}* and *Brca2^{+/SA}* cells was not impaired (Figures 6E and S4F). Furthermore, heterozygous *Brca2^{Δ27/+}* cells with defective RGS and SFP also reprogrammed with the efficiency of wild-type controls (Figure 6F), while homozygous *Brca2^{Δ27/Δ27}* mutants lacking all three functions HDR, RGS, and SFP⁵⁷ failed to reprogram.

DISCUSSION

The mechanisms safeguarding cellular identity are an important question in developmental biology. Previous reprogramming studies have identified histone and DNA methylation, chromatin

assembly factors, and posttranslational modifications as important determinants of iPSC formation.⁵⁸ While most studies have focused on barriers to changes in gene expression, there is mounting evidence that the DNA damage response and cell cycle checkpoints play a key role in safeguarding the somatic state. Somatic cell reprogramming results in increased DNA damage, as manifested by elevated γ H2AX nuclear foci.^{2,3,5} In the context of somatic cell nuclear transfer, DNA damage is acquired during DNA replication, starting from the first cell cycle.⁵ During iPSC reprogramming, γ H2AX foci are elevated no later than 4 days after reprogramming factor induction and remain elevated for at least 2 weeks.^{2,3} Thus, DNA damage and repair throughout the reprogramming process can have an impact on the formation and quality of the resulting iPSCs. Notably, *BRCA1*-mutant iPSC lines can be established at a reduced rate, suggesting that the requirement for BRCA1 is greater during the reprogramming process than in stable somatic and iPSC cultures.

Pathogenic *BRCA1* lesions tested prior to this study each abrogate all three of the primary mechanisms by which BRCA1 preserves genome integrity: HDR,¹³ SFP,¹⁷ and RGS.^{23,24} Here, we used separation-of-function mutations and genetic rescue experiments to ascertain the dependence of somatic cell reprogramming on each of these BRCA1 functions.

To specifically interrogate the relevance of SFP and RGS in iPSC generation, we examined different genotypes that abrogate SFP while leaving HDR intact, including heterozygous *Brca1^{tr/+}* mutants and cells that are either homozygous or heterozygous for the *Bard1* mutations *Bard1^{K607A}* or *Bard1^{S563F}*. Although these cells all display an HDR⁺SFP⁻ phenotype, each underwent reprogramming at efficiencies comparable to those of wild-type controls. Conversely, while loss of the DNA translocase SMARCAL1 restored SFP but not HDR function in *Brca1* mutants, reprogramming remained compromised. Together, these results rule out a major requirement for SFP in somatic cell reprogramming. Notably, *BRCA2^{SA}* mutant cells, which are deficient in RGS and SFP,⁵⁷ displayed a normal reprogramming potential, providing support for the notion that neither RGS nor SFP is limiting for reprogramming. By contrast, in all settings tested, reprogramming efficiency was highly sensitive to changes in HDR efficiency.

Although somatic cell reprogramming is accompanied by elevated formation of DSBs,^{2–5} the nature and origin of these breaks remain poorly understood. A distinction between one-ended and two-ended DSBs can be made based on their mechanism of formation and the genetic requirements for their repair. Two-ended DSBs can be repaired productively by either NHEJ or HDR. One-ended DSBs, which are generated primarily during S-phase through processing of collapsed replication forks and through forks encountering ssDNA breaks,^{45,46,59} are preferentially repaired by HDR. In this context, *53BP1* mutations, by favoring HDR over NHEJ repair, would be expected to enhance iPSC formation. Indeed, we observed that the reprogramming of *53bp1^{-/-}* fibroblasts was less sensitive to inducers of one-ended DSBs compared to wild-type cells, but was more vulnerable to two-ended DSBs generated by IR. This is consistent with the sensitivity of *53bp1^{-/-}* mice and embryonic cells to IR.⁵⁵ These results collectively indicate that the limiting factor

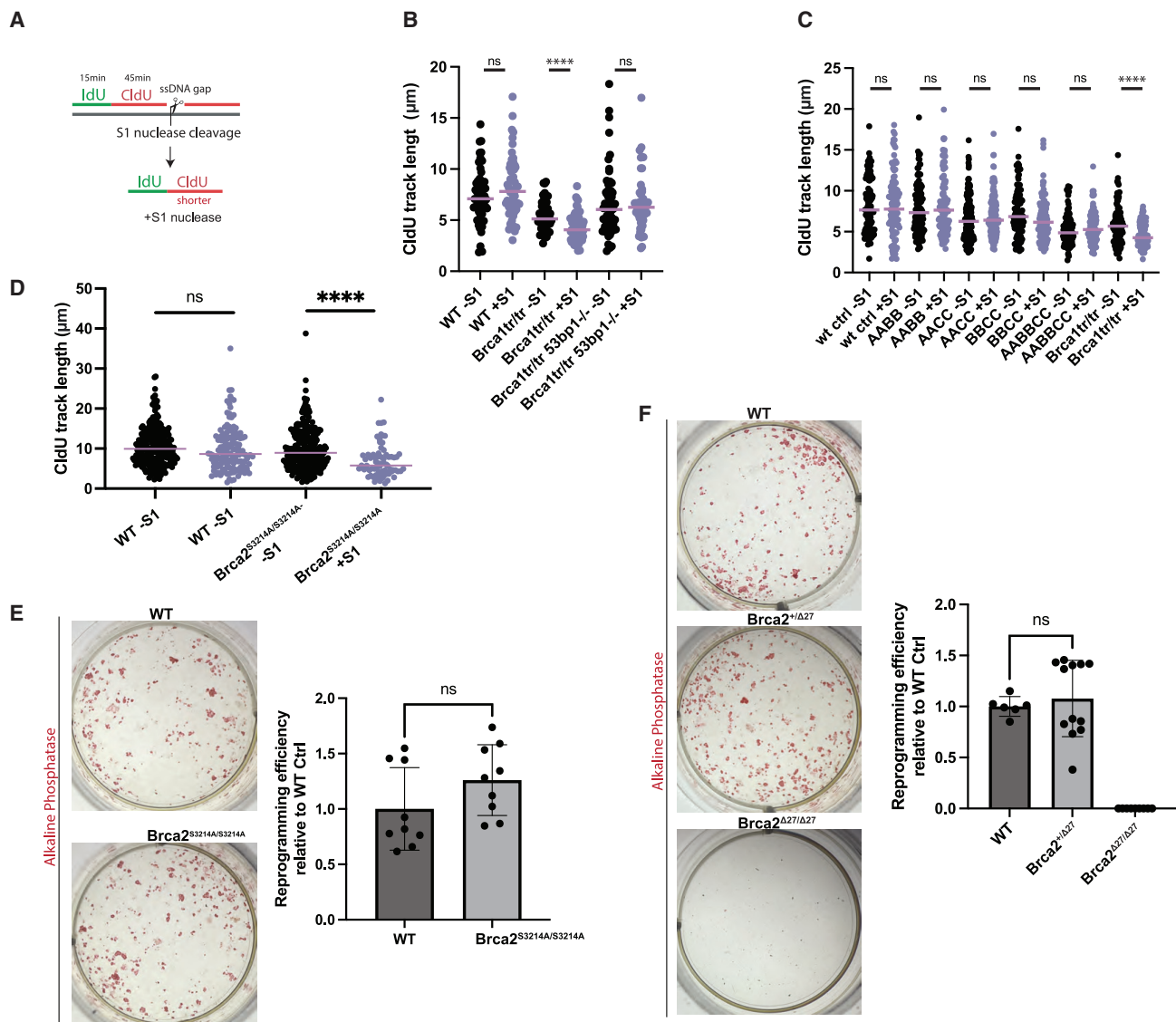


Figure 6. Replication gap suppression is not required for reprogramming

(A) Schematic of replication gap evaluation with S1 nuclease.

(B) Dot plot of CldU track length in iPSC lines of the indicated genotypes; ≥ 100 fibers were measured per experimental condition. Analysis by a two-tailed Mann-Whitney test. Median track length is marked by a purple line.

(C) Dot plot of CldU track length in iPSC lines of the indicated genotypes, collected from ≥ 50 fibers per condition and analyzed by a two-tailed Mann-Whitney test.

(D) Dot plot of CldU track length on reprogramming day 5 of the indicated genotypes; ≥ 100 fibers were measured per experimental condition. Analysis by a two-tailed Mann-Whitney test.

(E) AP staining and reprogramming efficiency quantification. The number of AP-positive colonies is shown relative to WT. Analysis was performed with an unpaired, two-tailed Student's t test; $n = 10$ for each genotype.

(F) AP staining and reprogramming efficiency quantification. The number of AP-positive colonies is shown as a ratio to WT. WT $n = 6$, *Brca2*^{Δ27/Δ27} $n = 12$, *Brca2*^{Δ271/Δ27} $n = 9$. Analysis by one-way ANOVA.

See also Figure S4.

for reprogramming to pluripotency is a replication-associated DSB, which requires repair by HDR.

A recent study has shown that, among these three functions (HDR, SFP, and RGS) of the BRCA2 tumor suppressor, HDR is the most significant contributor to genome stability and chemotherapeutic sensitivity in the context of cancer.⁵⁷ Likewise,

among these separable BRCA1/2 functions, we show here that HDR efficiency is also the most significant determinant of efficient iPSC reprogramming. Previous studies have pointed out additional genetic parallels between reprogramming and tumorigenesis,^{9,60} showing that reprogramming is facilitated by the loss of tumor suppressors that orchestrate the response to

unrepaired DNA damage, such as p53,⁹ p21,¹¹ or Rb.¹² As for tumor formation, replication-associated DNA damage is a barrier in the transition of somatic cells to the pluripotent state.^{3,5,61} In this study, we demonstrate that DSBs formed during DNA replication can suppress somatic cell reprogramming and that their proper resolution by the HDR pathway is essential for efficient iPSC generation. In the absence of HDR, unresolved DNA repair intermediates can persist through G2 into mitosis and the next G1,⁶² during which the retained damage suppresses further cell-cycle progression through activation of p53, p21, and Rb.^{63,64} Interestingly, p21 and Rb both have inhibitory consequences on OSKM-mediated transcriptional reprogramming, repressing expression of pluripotency factors and promoting maintenance of repressive histone marks.¹² Therefore, by affecting both cell-cycle progression and transcriptional reprogramming, an unrepaired replication-associated DSB inhibits iPSC formation. While a mutation in p53, p21, or Rb might improve reprogramming efficiency by decreasing the response to DNA damage, 53BP1 knockout increases reprogramming efficiency by enhancing HDR, the repair pathway most relevant to reprogramming. Inhibiting 53BP1 might thus be safer than checkpoint interference for the purpose of increasing reprogramming efficiency.

Reduced reprogramming efficiency is one consequence of genome instability, but *de novo* mutations and alterations in chromatin modifications or architecture may be another product of DNA replication stress. Replication stress during reprogramming contributes to copy-number changes,⁶⁵ compromising the utility of iPSCs in research and therapy, and has indeed adversely affected an autologous cell therapy trial.⁶⁶ Future studies should thus aim to determine the importance of different repair pathways in affecting the quality of the resulting iPSCs, including their genetic integrity and developmental potential.

Limitations of study

This study does not currently determine the impact of different DNA repair mechanisms on the quality of the resulting iPSC lines. The study also does not distinguish the temporal requirements of different repair pathways during somatic cell reprogramming. Furthermore, the conclusion that the one-ended DSB is the DNA lesion primarily responsible for affecting reprogramming efficiency is inferred from the genetic requirements of efficient reprogramming and is not directly determined by methods that can visualize these breaks directly.

STAR★METHODS

Detailed methods are provided in the online version of this paper and include the following:

- KEY RESOURCES TABLE
- RESOURCE AVAILABILITY
 - Lead contact
 - Materials availability
 - Data and code availability
- EXPERIMENTAL MODEL AND STUDY PARTICIPANT DETAILS
 - Animals

- Mouse embryonic fibroblasts
- Mouse iPSC lines
- Human cell lines
- METHOD DETAILS
 - Virus preparation and infection
 - Reprogramming
 - RT-qPCR, western blot, and immunofluorescence
 - DNA fiber analysis
 - HDR assay
 - Proliferation and apoptosis
 - Nanog detection
 - S1 nuclease assay
- QUANTIFICATION AND STATISTICAL ANALYSIS

SUPPLEMENTAL INFORMATION

Supplemental information can be found online at <https://doi.org/10.1016/j.celrep.2024.114006>.

ACKNOWLEDGMENTS

We thank Jean Gautier and Claudia Doege for comments and experimental suggestions; Thomas Ludwig for generating and providing the *Abraxas*^{S404A} and *Bach1*^{S994A} single-mutant mouse strains, which are being used for independent studies on tumorigenesis; Foon Wu-Baer and David Billing for sharing mouse strains and MEF lines; and Silvia Alvarez Nanez for training in DNA fiber analysis. This study was supported primarily by NIH/NIGMS 1R01GM132604-01A1 (D.E.) and also by NIH/NHGRI R21 HG010165-01A1 (D.E.), NYSTEM IDEA award C32564GG (D.E.); NIH/NCI R01CA197774 (A.C.), NIH/NCI R01CA227450 (A.C. and R.B.), NIH/NCI P01CA174653 (A.C. and R.B.), and NIH R35CA253174 (M.J.); the Diabetes Research Center Flow Core Facility Center grant P30DK063608; and Flow Cytometry Core Facility grant gg015965-01 5r01gm132604-02. C.R.R. was supported by fellowships from the National Cancer Institute (T32-CA09503) and the DoD Breast Cancer Research Program (BC083089). M.H. was supported by the JSPS Overseas Research Fellowship (JSPS-2016180) and the Uehara Memorial Foundation Research Fellowship (201740041).

AUTHOR CONTRIBUTIONS

D.G. and D.E. designed the experiments. D.G. bred all *Brca1*/*Smarcal1*/*53bp1*, *Bard1*, and *ABC* mouse genotypes and performed molecular analyses, including SFP and HDR assays, focus formation, proliferation/apoptosis, and reprogramming efficiency. N.W. performed studies on the role of RGS and human iPSC reprogramming, while contributing to other figures. D.G. and N.W. also measured the effects of replication inhibitors during reprogramming. S.J. and J.S. performed reprogramming experiments for manuscript revision, Q.D. performed qPCR for p21. A.T. and A.C. provided mice and critical input. A.T. and M.H. performed DNA fiber analysis on *Brca1*^{trf/+} and *ABC* immortalized MEFs. C.R.R. generated mice with *Abraxas*^{S404A}, *Bach1*^{S994A}, and *Ctip*^{S326A} mutant alleles. J.S. performed immunofluorescence. M.J. and P.X.L. generated the *Brca2*^{SA} MEFs and provided input on the study. D.G. analyzed data, created the figures, and wrote the manuscript with contributions from N.W., R.B., and D.E., the latter also providing supervision.

DECLARATION OF INTERESTS

D.G. and D.E. have applied for a patent on interfering with 53BP1 during somatic cell reprogramming.

Received: February 26, 2023

Revised: November 26, 2023

Accepted: March 11, 2024

REFERENCES

- Takahashi, K., and Yamanaka, S. (2006). Induction of pluripotent stem cells from mouse embryonic and adult fibroblast cultures by defined factors. *Cell* 126, 663–676.
- González, F., Georgieva, D., Vanoli, F., Shi, Z.D., Stadtfeld, M., Ludwig, T., Jasin, M., and Huangfu, D. (2013). Homologous recombination DNA repair genes play a critical role in reprogramming to a pluripotent state. *Cell Rep.* 3, 651–660. <https://doi.org/10.1016/j.celrep.2013.02.005>.
- Ruiz, S., Lopez-Contreras, A.J., Gabut, M., Marion, R.M., Gutierrez-Martinez, P., Bua, S., Ramirez, O., Olalde, I., Rodrigo-Perez, S., Li, H., et al. (2015). Limiting replication stress during somatic cell reprogramming reduces genomic instability in induced pluripotent stem cells. *Nat. Commun.* 6, 8036. <https://doi.org/10.1038/ncomms9036>.
- Müller, L.U.W., Milsom, M.D., Harris, C.E., Vyas, R., Brumme, K.M., Parmar, K., Moreau, L.A., Schambach, A., Park, I.H., London, W.B., et al. (2012). Overcoming reprogramming resistance of Fanconi anemia cells. *Blood* 119, 5449–5457. <https://doi.org/10.1182/blood-2012-02->
- Chia, G., Agudo, J., Treff, N., Sauer, M.V., Billing, D., Brown, B.D., Baer, R., and Egli, D. (2017). Genomic instability during reprogramming by nuclear transfer is DNA replication dependent. *Nat. Cell Biol.* 19, 282–291. <https://doi.org/10.1038/ncb3485>.
- Gómez-Cabello, D., Checa-Rodríguez, C., Abad, M., Serrano, M., and Huertas, P. (2017). CtIP-Specific Roles during Cell Reprogramming Have Long-Term Consequences in the Survival and Fitness of Induced Pluripotent Stem Cells. *Stem Cell Rep.* 8, 432–445. <https://doi.org/10.1016/j.stemcr.2016.12.009>.
- Raya, A., Rodríguez-Pizà, I., Guenechea, G., Vassena, R., Navarro, S., Barrero, M.J., Consiglio, A., Castellà, M., Río, P., Sleep, E., et al. (2009). Disease-corrected haematopoietic progenitors from Fanconi anaemia induced pluripotent stem cells. *Nature* 460, 53–59.
- Kinoshita, T., Nagamatsu, G., Kosaka, T., Takubo, K., Hotta, A., Ellis, J., and Suda, T. (2011). Ataxia-telangiectasia mutated (ATM) deficiency decreases reprogramming efficiency and leads to genomic instability in iPS cells. *Biochem. Biophys. Res. Commun.* 407, 321–326. <https://doi.org/10.1016/j.bbrc.2011.03.013>.
- Utikal, J., Polo, J.M., Stadtfeld, M., Maherali, N., Kulalert, W., Walsh, R.M., Khalil, A., Rheinwald, J.G., and Hochedlinger, K. (2009). Immortalization eliminates a roadblock during cellular reprogramming into iPS cells. *Nature* 460, 1145–1148. <https://doi.org/10.1038/nature08285>.
- Hong, H., Takahashi, K., Ichisaka, T., Aoi, T., Kanagawa, O., Nakagawa, M., Okita, K., and Yamanaka, S. (2009). Suppression of Induced Pluripotent Stem Cell Generation by the p53–p21 Pathway. *Nature* 460, 1132–1134.
- Kawamura, T., Suzuki, J., Wang, Y.V., Menendez, S., Morera, L.B., Raya, A., Wahi, G.M., and Izpisua Belmonte, J.C. (2009). Linking the p53 tumour suppressor pathway to somatic cell reprogramming. *Nature* 460, 1140–1144.
- Kareta, M.S., Gorges, L.L., Hafeez, S., Benayoun, B.A., Marro, S., Zmoos, A.F., Cecchini, M.J., Spacek, D., Batista, L.F.Z., O'Brien, M., et al. (2015). Inhibition of pluripotency networks by the Rb tumor suppressor restricts reprogramming and tumorigenesis. *Cell Stem Cell* 16, 39–50. <https://doi.org/10.1016/j.stem.2014.10.019>.
- Moynahan, M.E., Chiu, J.W., Koller, B.H., and Jasin, M. (1999). Brca1 Controls Homology-Directed DNA Repair. *Mol. Cell* 4, 511–518.
- Chen, C.C., Feng, W., Lim, P.X., Kass, E.M., and Jasin, M. (2018). Homology-Directed Repair and the Role of BRCA1, BRCA2, and Related Proteins in Genome Integrity and Cancer. *Annu. Rev. Cell Biol.* 2, 313–336. <https://doi.org/10.1146/annurev-cancerbio-030617-050502>.
- Bunting, S.F., Callén, E., Wong, N., Chen, H.T., Polato, F., Gunn, A., Bothmer, A., Feldhahn, N., Fernandez-Capetillo, O., Cao, L., et al. (2010). 53BP1 inhibits homologous recombination in Brca1-deficient cells by blocking resection of DNA breaks. *Cell* 141, 243–254. <https://doi.org/10.1016/j.cell.2010.03.012>.
- Setiawati, D., and Durocher, D. (2019). Shieldin - the protector of DNA ends. *EMBO Rep.* 20, e47560. <https://doi.org/10.15252/embr.201847560>.
- Schlacher, K., Wu, H., and Jasin, M. (2012). A distinct replication fork protection pathway connects Fanconi anemia tumor suppressors to RAD51-BRCA1/2. *Cancer Cell* 22, 106–116. <https://doi.org/10.1016/j.ccr.2012.05.015>.
- Pathania, S., Bade, S., Le Guillou, M., Burke, K., Reed, R., Bowman-Colin, C., Su, Y., Ting, D.T., Polyak, K., Richardson, A.L., et al. (2014). BRCA1 haploinsufficiency for replication stress suppression in primary cells. *Nat. Commun.* 5, 5496. <https://doi.org/10.1038/ncomms6496>.
- Billing, D., Horiguchi, M., Wu-Baer, F., Tagliatalata, A., Leuzzi, G., Nanez, S.A., Jiang, W., Zha, S., Szabolcs, M., Lin, C.S., et al. (2018). The BRCT Domains of the BRCA1 and BARD1 Tumor Suppressors Differentially Regulate Homology-Directed Repair and Stalled Fork Protection. *Mol. Cell* 72, 127–139.e8. <https://doi.org/10.1016/j.molcel.2018.08.016>.
- Mason, J.M., Chan, Y.L., Weichselbaum, R.W., and Bishop, D.K. (2019). Non-enzymatic roles of human RAD51 at stalled replication forks. *Nat. Commun.* 10, 4410. <https://doi.org/10.1038/s41467-019-12297-0>.
- Przetocka, S., Porro, A., Bolck, H.A., Walker, C., Lezaja, A., Trenner, A., von Aesch, C., Himmels, S.F., D'Andrea, A.D., Ceccaldi, R., et al. (2018). CtIP-Mediated Fork Protection Synergizes with BRCA1 to Suppress Genomic Instability upon DNA Replication Stress. *Mol. Cell* 72, 568–582.e6. <https://doi.org/10.1016/j.molcel.2018.09.014>.
- Schlacher, K., Christ, N., Siaud, N., Egashira, A., Wu, H., and Jasin, M. (2011). Double-strand break repair-independent role for BRCA2 in blocking stalled replication fork degradation by MRE11. *Cell* 145, 529–542. <https://doi.org/10.1016/j.cell.2011.03.041>.
- Tagliatalata, A., Leuzzi, G., Sannino, V., Cuella-Martin, R., Huang, J.W., Wu-Baer, F., Baer, R., Costanzo, V., and Ciccica, A. (2021). REV1-Polzeta maintains the viability of homologous recombination-deficient cancer cells through mutagenic repair of PRIMPOL-dependent ssDNA gaps. *Mol. Cell* 81, 4008–4025.e7. <https://doi.org/10.1016/j.molcel.2021.08.016>.
- Panzarino, N.J., Kraus, J.J., Cong, K., Peng, M., Mosqueda, M., Nayak, S.U., Bond, S.M., Calvo, J.A., Doshi, M.B., Bere, M., et al. (2020). Replication Gaps Underlie BRCA-deficiency and Therapy Response. *Cancer Res.* 81, 1388–1397. <https://doi.org/10.1158/0008-5472.CAN-20-1602>.
- Kang, Z., Fu, P., Alcivar, A.L., Fu, H., Redon, C., Foo, T.K., Zuo, Y., Ye, C., Baxley, R., Madireddy, A., et al. (2021). BRCA2 associates with MCM10 to suppress PRIMPOL-mediated repriming and single-stranded gap formation after DNA damage. *Nat. Commun.* 12, 5966. <https://doi.org/10.1038/s41467-021-26227-6>.
- Quinet, A., Tirman, S., Jackson, J., Šviković, S., Lemaçon, D., Carvajal-Maldonado, D., González-Acosta, D., Vessoni, A.T., Cybulla, E., Wood, M., et al. (2020). PRIMPOL-Mediated Adaptive Response Suppresses Replication Fork Reversal in BRCA-Deficient Cells. *Mol. Cell* 77, 461–474.e9. <https://doi.org/10.1016/j.molcel.2019.10.008>.
- Ludwig, T., Fisher, P., Ganesan, S., and Efstratiadis, A. (2001). Tumorigenesis in mice carrying a truncating Brca1 mutation. *Genes Dev.* 15, 1188–1193. <https://doi.org/10.1101/gad.879201>.
- Shakya, R., Reid, L.J., Reczek, C.R., Cole, F., Egli, D., Lin, C.S., deRooij, D.G., Hirsch, S., Ravi, K., Hicks, J.B., et al. (2011). BRCA1 Tumor Suppression Depends on BRCT Phosphoprotein Binding, But Not Its E3 Ligase Activity. *Science* 334, 525–528.
- Wang, B., Matsuo, S., Ballif, B.A., Zhang, D., Smogorzewska, A., Gygi, S.P., and Elledge, S.J. (2007). Abraxas and RAP80 form a BRCA1 protein complex required for the DNA damage response. *Science* 316, 1194–1198. <https://doi.org/10.1126/science.1139476>.
- Cantor, S.B., Bell, D.W., Ganesan, S., Kass, E.M., Drapkin, R., Grossman, S., Wahner, D.C., Sgroi, D.C., Lane, W.S., Haber, D.A., and Livingston, D.M. (2001). BACH1, a Novel Helicase-like Protein, Interacts Directly with BRCA1 and Contributes to Its DNA Repair Function. *Cell* 105, 149–160.

31. Yu, X., Wu, L.C., Bowcock, A.M., Aronheim, A., and Baer, R. (1998). The C-terminal (BRCT) Domains of BRCA1 Interact *In Vivo* with CtIP, a Protein Implicated in the CtBP Pathway of Transcriptional Repression. *J. Biol. Chem.* *273*, 25388–25392.
32. Mateos-Gomez, P.A., Kent, T., Deng, S.K., McDevitt, S., Kashkina, E., Hoang, T.M., Pomerantz, R.T., and Sfeir, A. (2017). The helicase domain of Poltheta counteracts RPA to promote alt-NHEJ. *Nat. Struct. Mol. Biol.* *24*, 1116–1123. <https://doi.org/10.1038/nsmb.3494>.
33. Wu, L.C., Wang, Z.W., Tsan, J.T., Spillman, M.A., Phung, A., Xu, X.L., Yang, M.C., Hwang, L.Y., Bowcock, A.M., and Baer, R. (1996). Identification of a RING protein that can interact *in vivo* with the BRCA1 gene product. *Nat. Genet.* *14*, 430–440.
34. Li, M., and Yu, X. (2013). Function of BRCA1 in the DNA damage response is mediated by ADP-ribosylation. *Cancer Cell* *23*, 693–704. <https://doi.org/10.1016/j.ccr.2013.03.025>.
35. Vassin, V.M., Anantha, R.W., Sokolova, E., Kanner, S., and Borowiec, J.A. (2009). Human RPA phosphorylation by ATR stimulates DNA synthesis and prevents ssDNA accumulation during DNA-replication stress. *J. Cell Sci.* *122*, 4070–4080. <https://doi.org/10.1242/jcs.053702>.
36. Murphy, A.K., Fitzgerald, M., Ro, T., Kim, J.H., Rabinowitsch, A.I., Chowdhury, D., Schildkraut, C.L., and Borowiec, J.A. (2014). Phosphorylated RPA recruits PALB2 to stalled DNA replication forks to facilitate fork recovery. *J. Cell Biol.* *206*, 493–507. <https://doi.org/10.1083/jcb.201404111>.
37. Joseph, S.A., Tagliatalata, A., Leuzzi, G., Huang, J.W., Cuella-Martin, R., and Ciccio, A. (2020). Time for remodeling: SNF2-family DNA translocases in replication fork metabolism and human disease. *DNA Repair* *95*, 102943. <https://doi.org/10.1016/j.dnarep.2020.102943>.
38. Tagliatalata, A., Alvarez, S., Leuzzi, G., Sannino, V., Ranjha, L., Huang, J.W., Madubata, C., Anand, R., Levy, B., Rabadan, R., et al. (2017). Restoration of Replication Fork Stability in BRCA1- and BRCA2-Deficient Cells by Inactivation of SNF2-Family Fork Remodelers. *Mol. Cell* *68*, 414–430.e8. <https://doi.org/10.1016/j.molcel.2017.09.036>.
39. Rodriguez, R., Müller, S., Yeoman, J.A., Trentesaux, C., Riou, J.F., and Balasubramanian, S. (2008). A novel small molecule that alters shelterin integrity and triggers a DNA-damage response at telomeres. *J. Am. Chem. Soc.* *130*, 15758–15759. <https://doi.org/10.1021/ja805615w>.
40. Mirman, Z., and de Lange, T. (2020). 53BP1: a DSB escort. *Genes Dev.* *34*, 7–23. <https://doi.org/10.1101/gad.333237>.
41. Bouwman, P., Aly, A., Escandell, J.M., Pieterse, M., Bartkova, J., van der Gulden, H., Hiddingh, S., Thanasoula, M., Kulkarni, A., Yang, Q., et al. (2010). 53BP1 loss rescues BRCA1 deficiency and is associated with triple-negative and BRCA-mutated breast cancers. *Nat. Struct. Mol. Biol.* *17*, 688–695. <https://doi.org/10.1038/nsmb.1831>.
42. Liu, W., Krishnamoorthy, A., Zhao, R., and Cortez, D. (2020). Two replication fork remodeling pathways generate nuclease substrates for distinct fork protection factors. *Sci. Adv.* *6*, eabc3598. <https://doi.org/10.1126/sciadv.abc3598>.
43. Cuella-Martin, R., Oliveira, C., Lockstone, H.E., Snellenberg, S., Grolmussova, N., and Chapman, J.R. (2016). 53BP1 Integrates DNA Repair and p53-Dependent Cell Fate Decisions via Distinct Mechanisms. *Mol. Cell* *64*, 51–64. <https://doi.org/10.1016/j.molcel.2016.08.002>.
44. Ward, I.M., Difilippantonio, S., Minn, K., Mueller, M.D., Molina, J.R., Yu, X., Frisk, C.S., Ried, T., Nussenzweig, A., and Chen, J. (2005). 53BP1 cooperates with p53 and functions as a haploinsufficient tumor suppressor in mice. *Mol. Cell Biol.* *25*, 10079–10086. <https://doi.org/10.1128/MCB.25.22.10079-10086.2005>.
45. Balestrini, A., Ristic, D., Dionne, I., Liu, X.Z., Wyman, C., Wellinger, R.J., and Petrini, J.H.J. (2013). The Ku heterodimer and the metabolism of single-ended DNA double-strand breaks. *Cell Rep.* *3*, 2033–2045. <https://doi.org/10.1016/j.celrep.2013.05.026>.
46. Shao, R.G., Cao, C.X., Zhang, H., Kohn, K.W., Wold, M.S., and Pommier, Y. (1999). Replication-mediated DNA damage by camptothecin induces phosphorylation of RPA by DNA-dependent protein kinase and dissociates RPA:DNA-PK complexes. *EMBO J.* *18*, 1397–1406. <https://doi.org/10.1093/emboj/18.5.1397>.
47. Strumberg, D., Pilon, A.A., Smith, M., Hickey, R., Malkas, L., and Pommier, Y. (2000). Conversion of topoisomerase I cleavage complexes on the leading strand of ribosomal DNA into 5'-phosphorylated DNA double-strand breaks by replication runoff. *Mol. Cell Biol.* *20*, 3977–3987. <https://doi.org/10.1128/mcb.20.11.3977-3987.2000>.
48. Rothkamm, K., Krüger, I., Thompson, L.H., and Löbrich, M. (2003). Pathways of DNA double-strand break repair during the mammalian cell cycle. *Mol. Cell Biol.* *23*, 5706–5715.
49. Glover, T.W., Berger, C., Coyle, J., and Echo, B. (1984). DNA polymerase α inhibition by aphidicolin induces gaps and breaks at common fragile sites in human chromosomes. *Hum. Genet.* *67*, 136–142.
50. Doege, C.A., Inoue, K., Yamashita, T., Rhee, D.B., Travis, S., Fujita, R., Guarnieri, P., Bhagat, G., Vanti, W.B., Shih, A., et al. (2012). Early-stage epigenetic modification during somatic cell reprogramming by Parp1 and Tet2. *Nature* *488*, 652–655. <https://doi.org/10.1038/nature11333>.
51. Farmer, H., McCabe, N., Lord, C.J., Tutt, A.N.J., Johnson, D.A., Richardson, T.B., Santarosa, M., Dillon, K.J., Hickson, I., Knights, C., et al. (2005). Targeting the DNA repair defect in BRCA mutant cells as a therapeutic strategy. *Nature* *434*, 917–921.
52. Bryant, H.E., Schultz, N., Thomas, H.D., Parker, K.M., Flower, D., Lopez, E., Kyle, S., Meuth, M., Curtin, N.J., and Helleday, T. (2005). Specific killing of BRCA2-deficient tumours with inhibitors of poly(ADP-ribose) polymerase. *Nature* *434*, 913–917.
53. Hanzlikova, H., Kalasova, I., Demin, A.A., Pennicott, L.E., Cihlarova, Z., and Caldecott, K.W. (2018). The Importance of Poly(ADP-Ribose) Polymerase as a Sensor of Unligated Okazaki Fragments during DNA Replication. *Mol. Cell* *71*, 319–331.e3. <https://doi.org/10.1016/j.molcel.2018.06.004>.
54. Cong, K., Peng, M., Kousholt, A.N., Lee, W.T.C., Lee, S., Nayak, S., Kraus, J., VanderVere-Carozza, P.S., Pawelczak, K.S., Calvo, J., et al. (2021). Replication gaps are a key determinant of PARP inhibitor synthetic lethality with BRCA deficiency. *Mol. Cell* *81*, 3128–3144.e7. <https://doi.org/10.1016/j.molcel.2021.06.011>.
55. Ward, I.M., Minn, K., van Deursen, J., and Chen, J. (2003). p53 Binding protein 53BP1 is required for DNA damage responses and tumor suppression in mice. *Mol. Cell Biol.* *23*, 2556–2563.
56. Quinet, A., Martins, D.J., Vessoni, A.T., Biard, D., Sarasin, A., Sary, A., and Menck, C.F.M. (2016). Translesion synthesis mechanisms depend on the nature of DNA damage in UV-irradiated human cells. *Nucleic Acids Res.* *44*, 5717–5731. <https://doi.org/10.1093/nar/gkw280>.
57. Lim, P.X., Zaman, M., Feng, W., and Jasin, M. (2024). BRCA2 promotes genomic integrity and therapy resistance primarily through its role in homology-directed repair. *Mol. Cell* *84*, 447–462.e10. <https://doi.org/10.1016/j.molcel.2023.12.025>.
58. Brumbaugh, J., Di Stefano, B., and Hochedlinger, K. (2019). Reprogramming: identifying the mechanisms that safeguard cell identity. *Development* *146*, dev182170. <https://doi.org/10.1242/dev.182170>.
59. Ryan, A.J., Squires, S., Strutt, H.L., and Johnson, R.T. (1991). Camptothecin cytotoxicity in mammalian cells is associated with the induction of persistent double strand breaks in replicating DNA. *Nucleic Acids Res.* *19*, 3295–3300. <https://doi.org/10.1093/nar/19.12.3295>.
60. Ben-Porath, I., Thomson, M.W., Carey, V.J., Ge, R., Bell, G.W., Regev, A., and Weinberg, R.A. (2008). An embryonic stem cell-like gene expression signature in poorly differentiated aggressive human tumors. *Nat. Genet.* *40*, 499–507. <https://doi.org/10.1038/ng.127>.
61. Bartkova, J., Rezaei, N., Liontos, M., Karakaidos, P., Kletsas, D., Issaeva, N., Vassiliou, L.V.F., Kolettas, E., Niforou, K., Zoumpouris, V.C., et al. (2006). Oncogene-induced senescence is part of the tumorigenesis barrier imposed by DNA damage checkpoints. *Nature* *444*, 633–637. <https://doi.org/10.1038/nature05268>.

62. Moreno, A., Carrington, J.T., Albergante, L., Al Mamun, M., Haagensen, E.J., Komseli, E.S., Gorgoulis, V.G., Newman, T.J., and Blow, J.J. (2016). Unreplicated DNA remaining from unperturbed S phases passes through mitosis for resolution in daughter cells. *Proc. Natl. Acad. Sci. USA* *113*, E5757–E5764. <https://doi.org/10.1073/pnas.1603252113>.
63. Lezaja, A., and Altmeyer, M. (2018). Inherited DNA lesions determine G1 duration in the next cell cycle. *Cell Cycle* *17*, 24–32. <https://doi.org/10.1080/15384101.2017.1383578>.
64. Moser, J., Miller, I., Carter, D., and Spencer, S.L. (2018). Control of the Restriction Point by Rb and p21. *Proc. Natl. Acad. Sci. USA* *115*, E8219–E8227. <https://doi.org/10.1073/pnas.1722446115>.
65. Hussein, S.M., Batada, N.N., Vuoristo, S., Ching, R.W., Autio, R., Närvä, E., Ng, S., Sourour, M., Hämmäläinen, R., Olsson, C., et al. (2011). Copy number variation and selection during reprogramming to pluripotency. *Nature* *471*, 58–62. <https://doi.org/10.1038/nature09871>.
66. Mandai, M., Watanabe, A., Kurimoto, Y., Hiram, Y., Morinaga, C., Daimon, T., Fujihara, M., Akimaru, H., Sakai, N., Shibata, Y., et al. (2017). Autologous Induced Stem-Cell-Derived Retinal Cells for Macular Degeneration. *N. Engl. J. Med.* *376*, 1038–1046. <https://doi.org/10.1056/NEJMoa1608368>.
67. Orlando, L., Tanasijevic, B., Nakanishi, M., Reid, J.C., García-Rodríguez, J.L., Chauhan, K.D., Porras, D.P., Aslostovar, L., Lu, J.D., Shapovalova, Z., et al. (2021). Phosphorylation state of the histone variant H2A.X controls human stem and progenitor cell fate decisions. *Cell Rep.* *34*, 108818. <https://doi.org/10.1016/j.celrep.2021.108818>.
68. Sui, L., Xin, Y., Du, Q., Georgieva, D., Diedenhofen, G., Haataja, L., Su, Q., Zuccaro, M.V., Kim, J., Fu, J., et al. (2021). Reduced replication fork speed promotes pancreatic endocrine differentiation and controls graft size. *JCI Insight* *6*, e141553. <https://doi.org/10.1172/jci.insight.141553>.
69. Reczek, C.R., Szabolcs, M., Stark, J.M., Ludwig, T., and Baer, R. (2013). The interaction between CtIP and BRCA1 is not essential for resection-mediated DNA repair or tumor suppression. *J. Cell Biol.* *201*, 693–707. <https://doi.org/10.1083/jcb.201302145>.
70. Durkin, M.E., Qian, X., Popescu, N.C., and Lowy, D.R. (2013). Isolation of Mouse Embryo Fibroblasts. *Bio. Protoc.* *3*, e908. <https://doi.org/10.21769/bioprotoc.908>.
71. Anantha, R.W., Vassin, V.M., and Borowiec, J.A. (2007). Sequential and synergistic modification of human RPA stimulates chromosomal DNA repair. *J. Biol. Chem.* *282*, 35910–35923. <https://doi.org/10.1074/jbc.M704645200>.
72. Palmerola, K.L., Amrane, S., De Los Angeles, A., Xu, S., Wang, N., de Pinho, J., Zuccaro, M.V., Tagliatela, A., Massey, D.J., Turocy, J., et al. (2022). Replication stress impairs chromosome segregation and preimplantation development in human embryos. *Cell* *185*, 2988–3007.e20. <https://doi.org/10.1016/j.cell.2022.06.028>.
73. Terret, M.E., Sherwood, R., Rahman, S., Qin, J., and Jallepalli, P.V. (2009). Cohesin acetylation speeds the replication fork. *Nature* *462*, 231–234. <https://doi.org/10.1038/nature08550>.

STAR★METHODS

KEY RESOURCES TABLE

REAGENT or RESOURCE	SOURCE	IDENTIFIER
Antibodies		
Sox2	Stemgent	Cat# 09-0024; RRID: AB_2195775
rabbit-p21	Abcam	Cat# ab188224; RRID :AB_2734729
rabbit α -alpha tubulin	Abcam	Cat# ab4074; RRID: AB_2288001
Anti-phospho-Histone H2A.X-Ser139 mouse monoclonal Ab. Does not react to S139A in human pluripotent stem cells (Orlando et al. ⁶⁷)	Millipore	Cat# 05-636; RRID: AB_309864
rabbit α phospho-RPA2Ser33	Invitrogen	Cat# PA5-39809; RRID: AB_2556360
α 53BP1 H-300	Santa Cruz	Cat# 22760; RRID: AB_2256326
rabbit α Nanog	Reprocell	Cat#RCAB001P2P; RRID: AB_1560380
Alexa Fluor 488 conjugated mouse α human TRA-1-60	BD Biosciences	Cat# BD560173; RRID: AB_1645379
Purified mouse anti human 53BP1, clone 19	BD Transduction laboratories	Cat# 612522; RRID: AB_2206766
Anti-Rad51 (Ab-1) Rabbit pAb.	EMD Millipore	Cat# PC130, lot D00 138544; RRID: AB_2314029
Anti IdU antibody	BD Biosciences	Cat# BD 347580; RRID: AB_400326
Anti CldU antibody	Biorad	Cat# OBT0030; RRID: AB_2314029
Rat anti-BrdU	Abcam	Cat# ab6326; RRID: AB_2313786
Anti ssDNA antibody	Millipore	Cat# MAB3034; RRID: AB_11212688
Alexa Fluor 488 Donkey Anti-Rabbit IgG (H+L) Antibody	Thermo Fisher Scientific	Cat# A-21206; RRID: AB_3535792
Alexa Fluor 488 goat anti-mouse IgG1	Thermo Fisher Scientific	Cat# A-21121; RRID: AB_2535764
Alexa Fluor 488 goat anti-rat IgG	Thermo Fisher Scientific	Cat# A11007; RRID: AB_10561522
Alexa Fluor 488 goat anti-mouse IgG2a	Thermo Fisher Scientific	Cat# A21241; RRID: AB_2535810
Chemicals, peptides, and recombinant proteins		
DMEM-HG	Thermo Fisher Scientific	Cat#10569010
Knockout DMEM	Life Technologies	Cat# 10829-018
Stemflex	Gibco	Cat# A3349401
5-Iodo-2'-deoxyuridine (IdU)	Sigma Aldrich	Cat# I7125
5-Chloro-2'-deoxyuridine (CldU)	Sigma Aldrich	Cat# C6891
DMSO	Sigma Aldrich	Cat# D2650
PBS	Life Technologies	Cat# 14190-250
TrypLE Express	LifeTechnologies	12605036
Gelatin	Millipore	#ES-006-B
FBS	Atlanta Biologicals	Cat# S11150
Knockout Serum Replacement	Life Technologies	Cat# 10828-028
Glutamax	Thermo Fisher Scientific	Cat# 35050079
MEM NEAA	Life Technologies	Cat# 11140050
PenStrep	Thermo Fisher Scientific	Cat# 15140163
Jetprime	VWR	Cat# 89129-922
Protamine Sulfate	Fisher Scientific	Cat# 0219472905
Doxycycline	Sigma Aldrich	Cat# D9891
2-mercaptoetahnol	Life Technologies	Cat# 21985-023
LIF	eBioscience	Cat# 34-8521-82
Aphidicolin	Sigma Aldrich	Cat# A0781

(Continued on next page)

Continued

REAGENT or RESOURCE	SOURCE	IDENTIFIER
Topotecan	Sigma Aldrich	Cat# T2705
Olaparib	Selleckchem	Cat# S1060
Hydroxyurea	Sigma-Aldrich	Cat# H8627-1G
Pyridostatin	Selleck Chemicals	Cat# S7444
Puromycin	Thermo Fisher	Cat# A11138-03
Cell Trace CFSE proliferation dye	Thermo Fisher	Cat# C34554
Propidium Iodide	Millipore	Cat# 537059
HEPES	Sigma Aldrich	Cat# H4034
Fatty acid free BSA	Millipore Sigma	Cat# 126575
Acetic acid	LabChem	Cat# LC101003s
Methanol	Sigma Aldrich	Cat# 322415
Triton X-100	Sigma Aldrich	Cat# T8787
Ethylenediaminetetraacetic acid (EDTA)	Sigma Aldrich	Cat# E6758
Sodium dodecyl sulfate (SDS)	Sigma Aldrich	Cat# L3771
Tris base	Sigma Aldrich	Cat# T1503
NaCl	Sigma-Aldrich	Cat# 71376
MOPS	Sigma-Aldrich	Cat# M1254
MgCl ₂	Sigma-Aldrich	Cat# M7304
Sucrose	Sigma-Aldrich	Cat# S0389
HCl	Fisher Scientific	Cat# A144sl-212
S1 nuclease	Thermo Fisher Scientific	Cat# 18001-016
Acidic Tyrode's solution	EMD Millipore	Cat# MR-004-D
Prolong Gold Antifade	Thermo Fisher Scientific	Cat# P10144
Paraformaldehyde	Santa Cruz Biotechnology	Cat# sc-281692
Hoechst33342	Life Technologies	Cat# H3570

Critical commercial assays

Vector Red detection kit	Vector Laboratories	Cat# SK-5100
CytoTune-iPS 2.0 Sendai Reprogramming Kit	Thermo Fisher Scientific	Cat# A16517
RNeasy Mini Kit	Qiagen	Cat# 74104
iScript™ cDNA Synthesis Kit	Bio-RAD	Cat# 1708891
AzuraView™ GreenFast qPCR Blue Mix	Azura Genomics	Cat# AZ-2305
Annexin V-FITC apoptosis detection kit	Sigma Aldrich	Cat# APOAF-20TST

Experimental models: Cell lines

293T cells	ATCC	CRL-3216
MEFs: Brca2 ^{S3214A/S3214A}	Jasin lab, Memorial Sloan Kettering Cancer Center (Lim et al. ⁵⁷)	N/A
MEFs: Brca2 ^{+/Δ27}	Jasin lab, Memorial Sloan Kettering Cancer Center (Lim et al. ⁵⁷)	N/A
MEFs: Brca2 ^{Δ27/Δ27}	Jasin lab, Memorial Sloan Kettering Cancer Center (Lim et al. ⁵⁷)	N/A
MEFs: Brca2 ^{+/^{S3214A}}	Jasin lab, Memorial Sloan Kettering Cancer Center (Lim et al. ⁵⁷)	N/A
MEFs: Brca1 ^{tr/tr} Smarcal1 ^{+/-}	This paper	N/A
MEFs: Brca1 ^{tr/tr} Smarcal1 ^{-/-}	This paper	N/A
MEFs: Brca1 ^{tr/tr} 53bp1 ^{-/-}	This paper	N/A
MEFs: Brca1 ^{tr/tr} 53bp1 ^{+/-}	This paper	N/A
MEFs: Smarcal1 ^{+/-}	This paper	N/A
MEFs: Smarcal1 ^{-/-}	This paper	N/A
MEFs: Brca1 ^{tr/+}	This paper	N/A

(Continued on next page)

Continued

REAGENT or RESOURCE	SOURCE	IDENTIFIER
MEFs: Brca1 ^{tr/tr}	This paper	N/A
MEFs: 53bp1 ^{+/-}	This paper	N/A
MEFs: 53bp1 ^{-/-}	This paper	N/A
MEFs: AABB	This paper	N/A
MEFs: BBCC	This paper	N/A
MEFs: AACC	This paper	N/A
MEFs: AABBCC	This paper	N/A
MEFs: Bard1K607A/+	This paper	N/A
MEFs: Bard1K607A/K607A	This paper	N/A
MEFs: Bard1S563F/+	This paper	N/A
MEFs: Bard1S563F/S563F	This paper	N/A
Abraxas ^{S404A/S404A} Bach1 ^{S994A/S994A} iPSC (AABB iPSC)	This paper; Columbia University Medical Center	N/A
Bach1 ^{S994A/S994A} Ctip ^{S326A/S326A} iPSC (BBCC iPSC)	This paper; Columbia University Medical Center	N/A
Abraxas ^{S404A/S404A} Ctip ^{S326A/S326A} iPSC (AACC iPSC)	This paper; Columbia University Medical Center	N/A
Abraxas ^{S404A/S404A} Bach1 ^{S994A/S994A} Ctip ^{S326A/S326A} iPSC (AABBCC iPSC)	This paper; Columbia University Medical Center	N/A
Brca1 ^{tr/+} iPSC	This paper; Columbia University Medical Center	N/A
Brca1 ^{tr/tr} iPSC	This paper; Columbia University Medical Center	N/A
Brca1 ^{tr/tr} Smarcal1 ^{-/-} iPSC	This paper; Columbia University Medical Center	N/A
53bp1 ^{-/-} iPSC	This paper; Columbia University Medical Center	N/A
Brca1 ^{tr/tr} iPSC	This paper; Columbia University Medical Center	N/A
Brca1 ^{tr/tr} 53bp1 ^{+/-} iPSC	This paper; Columbia University Medical Center	N/A
Brca1 ^{tr/tr} 53bp1 ^{-/-} iPSC	This paper; Columbia University Medical Center	N/A
Human somatic cell line	Columbia University Medical Center, Egli lab repository, https://www.egliab.com/cell-line-repository (Sui et al. ⁶⁸)	#1-023

Experimental models: Organisms/strains

Mouse: C57BL/6J	The Jackson Laboratory	RRID: IMSR_JAX:000664
Mouse: Smarcal1 ^{+/-, +/-}	the International Mouse Phenotyping Consortium (IMPC)	N/A
Mouse: Bard1 ^{K607A/+, K607A/K607A, S563F/+, S563F/S563F, tr/+} (C57BL/6J)	This paper	N/A
Mouse: Brca1 ^{tr/tr, tr/+}	This paper	N/A
Mouse: Brca1 ^{tr/+, tr/tr} Smarcal1 ^{+/-, -/-} (C57BL/6J and 129Sv)	This paper	N/A
Mouse: Brca1 ^{tr/+, tr/tr} 53bp1 ^{+/-, -/-} (C57BL/6J and 129Sv)	This paper	N/A
Mouse: 53bp1 ^{+/-, -/-}	This paper	N/A
Mouse: Abraxas ^{S404A/S404A} (C57BL/6J and 129Sv)	This paper	N/A

(Continued on next page)

Continued		
REAGENT or RESOURCE	SOURCE	IDENTIFIER
Mouse: Ctip ^{S326A/S326A} (C57BL/6J and 129Sv)	Jackson Laboratories (Reczek et al. ⁶⁹)	RRID: IMSR_JAX:036502
Mouse: Bach1 ^{S994A/S994A} (C57BL/6J and 129Sv)	This paper	N/A
Oligonucleotides		
Primer: 53BP1 Forward: ATGGACCCTACTGGAAGTCAG	This paper	N/A
Primer: 53BP1 Reverse: TTTCTTTGTGCGTCTGGAGATT	This paper	N/A
Primer: GAPDH Forward: GGAGCGAGATCCCTCCAAAT	This paper	N/A
Primer: GAPDH Reverse: GGCTGTTGTCATACTTCTCATGG	This paper	N/A
Primer: P21 Forward: GCCTTAGCCCTCACTCTGTG	This paper	N/A
Primer: P21 Reverse: AGCTGGCCTTAGAGGTGACA	This paper	N/A
Primer: Beta actin Forward: GGCTGTATTCCCCTCCATCG	This paper	N/A
Primer: Beta actin Reverse: CCAGTTGGTAACAATGCCATGT	This paper	N/A
53BP1-siRNA	Sigma Aldrich	Cat#SASI_Hs01_00024577
Recombinant DNA		
pTet-O-FUW-OSKM	Addgene	Cat# 20321
pFUW-M2rtTA	Addgene	Cat# 20342
pMD2VSVG	Addgene	Cat# 12259
psPax2	Addgene	Cat# 12260
Software and algorithms		
Prism	GraphPad	https://www.graphpad.com/scientific-software/prism/
Zen confocal imaging and mage processing software	Zeiss	https://www.zeiss.com/microscopy/us/products/microscope-software/zen.html
Olympus cellSens imaging and analysis software	Olympus life science	https://www.olympus-lifescience.com/en/software/cellsens
FlowJo v.10	FlowJo	https://www.flowjo.com/solutions/flowjo/downloads
ImageJ software	ImageJ	https://imagej.net/ij/
Other		
40µm cell strainer	Fisher Scientific	Cat# 08-771-1
0.45µm PES Syringe Filters	CELLTREAT	Cat# 229749

RESOURCE AVAILABILITY

Lead contact

Further information and requests for resources and reagents should be directed to and will be fulfilled by the Lead Contact, Dieter Egli (de2220@cumc.columbia.edu).

Materials availability

Requests for iPSC lines or mice should be addressed to Dieter Egli. Columbia University requires the completion of an MTA for the distribution of materials.

Data and code availability

- Data reported in this paper will be shared by the [lead contact](#) upon request.
- This paper does not report original code.
- Any additional information required to reanalyze the data reported in this paper is available from the [lead contact](#) upon request.

EXPERIMENTAL MODEL AND STUDY PARTICIPANT DETAILS

Animals

All mouse experiments performed in this study are in compliance with ethical regulations regarding the use of research animals and were approved by the Columbia University IACUC. Animals are housed in a barrier facility in individually ventilated cages.

To generate *Bard1* mutants, heterozygous *Bard1*^{K607A/+} and *Bard1*^{S563F/+} females on a C57BL/6J background¹⁹ were bred to males of the same genotypes at ages 10–50 weeks of age. The *Brca1/Smcal1* genotype panel was created from intercrosses between *Brca1*^{tr/+}*Smcal1*^{+/-} animals of mixed C57BL/6J and 129Sv background. The *Brca1*^{tr/+} allele is described in Ludwig et al.²⁷ Mice mutant for *Smcal1* were obtained from the International Mouse Phenotyping Consortium (IMPC). The *Brca1/53bp1* genotype panel was generated from intercrosses between *Brca1*^{tr/+}*53bp1*^{+/-} males and females on a mixed C57BL/6J and 129Sv background. The *Abraxas/Bach/Ctip* genotype panel was also generated on a mixed background (C57BL/6J and 129Sv) by crossing homozygous *Ctip*^{S326A/S326A} mice⁶⁹ (designated here as “CC” mice and available from Jackson under strain #036502) with double homozygous *Abraxas*^{S404A/S404A}*Bach1*^{S994A/S994A} mice (kindly provided by Dr. Thomas Ludwig, Columbia University, and designated here as “AABB” mice). The F1 triple heterozygous (“A+B+C+”) progeny was then intercrossed to obtain the different combinations of double homozygous mutants. To generate triple homozygous *AABBCC* mice, the F2 *A+BBCC* males were crossed to F2 *A+BBCC* or *A+BBCC+* females. From the *A+BBCC* × *A+BBCC* crosses, 1 of 9 embryos was triple homozygous *AABBCC* (expected Mendelian ratio is 1/4). One additional *AABBCC* embryo was obtained from triple heterozygous intercrosses (*A+B+C+* × *A+B+C+*) that produced 69 embryos (expected Mendelian ratio is 1/64). *BRCA2*^{S3214A} (*BRCA2*^{SA}) mice and their characterization of SFP and RGS were described recently.⁵⁷

Mouse embryonic fibroblasts

To derive fibroblasts for reprogramming, we harvested E13.5 mouse embryos from the above described crosses and processed them as in Durkin et al.⁷⁰ with minor modifications. The cells from a single embryo were then plated in one 10cm dish and grown in MEF media, consisting of DMEM HG (Thermo Fisher Scientific #10569010), supplemented with 10% FBS (Atlanta Biologicals #S11150), Glutamax (Thermo Fisher Scientific #35050079) and PenStrep (Thermo Fisher Scientific 15140163). Cells were split once to P1 and frozen down for reprogramming experiments. The sequences of all genotyping primers are provided in [Table S3](#).

Mouse iPSC lines

A list of all mouse iPSC lines and their genotypes is provided in [Table S2](#). Methods for growing mouse iPSCs are provided in the Method details.

Human cell lines

Somatic human cells from an adult male (ID#1023) were used, available from a public cell repository (<https://www.ezlab.com/cell-line-repository>). All research with human cells was approved by the Columbia University Embryonic Stem Cell Research Oversight Committee and by the IRB.

METHOD DETAILS

Virus preparation and infection

This study used a doxycycline inducible lentiviral system, consisting of Tet-O-FUW-OSKM (Addgene #20321) and FUW-M2rtTA (Addgene # 20342). Lentivirus was prepared in 293T cells by transfection of plasmids with Jetprime transfection reagent (VWR #89129-922) as outlined in the manufacturer’s instructions. Briefly, Tet-O-FUW vectors were transfected together with the envelope and packaging plasmids from Didier Trono pMD2VSVG (Addgene #12259) and psPax2 (Addgene # 12260) into 293T cells plated on collagen-coated dishes. Fresh antibiotic-free media DMEM HG (Thermo Fisher Scientific #10569010), supplemented with 15% FBS (Atlanta Biologicals #S11150) and Glutamax (Thermo Fisher Scientific #35050079) was provided 16 to 20h post transfection. Viral supernatant was collected on each of the following two days and kept at 4°C for up to 4 days. Prior to infection, titer from the two collection days was pooled and filtered through a 40µm cell strainer (Fisher Scientific #08-771-1).

For infection, P1 mouse embryonic fibroblasts (MEFs) were thawed and plated at 1×10⁶ cells per 10cm dish on the previous day. Infection proceeded in two rounds with 8h to 9h in between. Briefly, cells were incubated with an OSKM/rtta virus mix (1:1), supplemented with 8ug/ml protamine sulfate (Fisher Scientific #0219472905). The infection mix was removed on the following day and cells were left to recover in fresh MEF media (DMEM HG Thermo Fisher Scientific #10569010 with 10% FBS Atlanta Biologicals #S11150, Glutamax Thermo Fisher Scientific #35050079 and PenStrep Thermo Fisher Scientific 15140163).

Reprogramming

Two days after infection, cells were re-plated on gelatin-coated dishes for transduction efficiency assessment on day 3, molecular analyses on day 5, colony picking on day 16 and alkaline phosphatase (AP) staining on day 20. In each experiment, infected fibroblasts from the different genotypes were re-plated at multiple densities to allow for optimal reprogramming efficiency. For wild-type cells, 100–300 cells/mm² (20–60K per well of a 24w dish) routinely generated high numbers of iPSC clones. Besides for wild type, 20–60K per well of a 24w dish was also optimal for the *Bard1* point mutants, *Brca1*^{tr/+} (and all combination mutations with *Smarca1* or *53bp1*), *Brca1*^{tr/tr}*53bp1*^{-/-} as well as the heterozygous or homozygous *Smarca1* and *53bp1* single mutants. The 3 genotypes-*Brca1*^{tr/tr}; *Brca1*^{tr/tr}*Smarca1*^{+/-} and *Brca1*^{tr/tr}*Smarca1*^{-/-} were plated at 600–800 cells/mm² (120,000–160,000 per well of a 24w dish) to obtain any reprogramming; we observed no iPSC clones at the densities selected for wild type for these genotypes. The *Brca1*^{tr/tr}*53bp1*^{+/-} genotype was re-plated at 450 cells/mm² (90K/well of a 24w dish). These seeding densities were used to calculate reprogramming efficiency of each genotype. Reprogramming experiments involving *Brca2*^{SA} and *Brca2*^{Δ27} genotypes and controls used blinding to sample identity and cells of all genotypes were seeded at 40K per well.

The OSKM reprogramming factors were induced with 1 μg/ml doxycycline (Sigma # D9891) in mouse embryonic stem (mES) cell media, consisting of Knockout DMEM (Life Technologies #10829-018), supplemented with 15% Knockout Serum Replacement (Life Technologies #10828-028), Glutamax (Thermo Fisher Scientific #35050079), MEM NEAA (Life Technologies #11140050), PenStrep (Thermo Fisher Scientific 15140163), 2-mercaptoethanol (Life Technologies #21985-023) and 10 ng/μL LIF (eBioscience #34-8521-82). Transduction efficiency was determined on reprogramming day 3 by staining for Sox2 (Stemgent #09-0024) and used in the calculation of reprogramming efficiency.

mES media was also used for routine culture of iPSC lines. Mouse iPSCs were maintained on a feeder layer of irradiated MEFs, plated on 0.1% gelatin-coated (Millipore #ES-006-B) tissue culture plates in standard miPSCs medium, consisting of Knockout DMEM (Life Technologies #10829-018), supplemented with 15% ESC grade FBS (Atlanta Biologicals #S11150), Glutamax (Thermo Fisher Scientific #35050079), MEM NEAA (Life Technologies #11140050), PenStrep (Thermo Fisher Scientific 15140163), 2-mercaptoethanol (Life Technologies #21985-023) and 10 ng/μL LIF (eBioscience #34-8521-82). Splitting was performed with TrypLE (Life Technologies).

The reprogramming experiments with drug treatment used aphidicolin (Sigma #A0781) at 0.2 μM, topotecan (Sigma #T2705) at 10 nM or olaparib at 50 nM (Selleckchem #S1060) for 8 days during reprogramming. Alternatively, for the induction of two-ended DSBs, cells were subjected to a single dose of 3 Gy or 6 Gy IR 1 day post doxycycline-mediated OSKM factor induction. Cells were fixed on reprogramming day 18–20 and stained for alkaline phosphatase with the Vector Red detection kit (Vector Laboratories #SK-5100). Reprogramming efficiency was determined by considering the number of AP-positive colonies per number of infected cells, determined by Sox2 staining at the optimal plating density for each genotype. The sensitivity score to drugs was obtained by calculating the ratio of treated wild type (normalized to untreated wild type) to treated mutant (normalized to untreated mutant). A high score represents greater sensitivity and lower reprogramming.

The reprogramming experiments with human cells used ID1023 dermal fibroblasts, from an adult male. To downregulate 53BP1, 1023 fibroblasts were transfected with 53BP1-siRNA (Sigma, SASI_Hs01_00024577) in Jetprime transfection reagent (VWR #89129-922), according to the manufacturer's instructions. Cells were harvested 48h post siRNA transfection for qPCR and WB. Three days after siRNA transfection, cells were transduced with sendai virus reprogramming vectors (hKOS, hc-Myc and hKlf4) from the CytoTune-iPS 2.0 Sendai Reprogramming Kit (Thermo Fisher Scientific #A16517) with a MOI as outlined in the manufacturer's protocol. On day 7 after sendai virus transduction, cells were re-plated on geltrex-coated 24-well dishes and from day 8 onward, were cultured in Stemflex medium (Gibco #A3349401).

RT-qPCR, western blot, and immunofluorescence

Total RNA from human fibroblasts (ID#1023) was extracted with the RNeasy Mini Kit (Qiagen #74104) according to the manufacturer's protocol. 1 μg of RNA was reverse-transcribed using the iScriptTM cDNA Synthesis Kit (Bio-RAD #1708891). The RT-qPCR reactions were prepared in triplicates with the AzuraViewTM GreenFast qPCR Blue Mix (Azura Genomics #AZ-2305) and the products were detected in a CFX96 real-time PCR system (Bio-Rad, Hercules, CA, USA). The reaction condition were: 95°C for 2min, and 40 cycles of 95°C for 5s and 60°C for 30 s. The relative expression level of genes was normalized to that of GAPDH and calculated using 2^{-ΔΔCt} method. The sequences of primers used in this study were:

53BP1 Forward: 5'-ATGGACCCTACTGGAAGTCAG
 53BP1 Reverse: 5'-TTTCTTTGTGCGTCTGGAGATT
 GAPD Forward: 5'-GGAGCGAGATCCCTCCAAAAT
 GAPDH Reverse: 5'-GGCTGTTGTCATACTTCTCATGG
 P21 Forward: 5'-GCCTTAGCCCTCACTCTGTG
 P21 Reverse: 5'-AGCTGGCCTTAGAGGTGACA
 Beta actin Forward: 5'-GGCTGTATTCCCCTCCATCG
 Beta actin Reverse: 5'-CCAGTTGGTAACAATGCCATGT

For p21 detection, protein was harvested from wild-type and *53bp1*-mutant uninfected MEFs as well as infected MEFs of the same genotypes on reprogramming day 5. Lysis was performed in RIPA buffer and proteins of interest were detected with the following

antibodies: rabbit α p21 (Abcam #ab188224) and rabbit α -alpha tubulin (Abcam #ab4074). 53BP1 was detected in human dermal fibroblasts 48h post siRNA transfection with mouse α 53BP1 (BD Biosciences #BD612522).

Detection of phospho-H2AX(S139), i.e. γ H2AX, phospho-RPA(S33) and 53bp1 was performed by immunofluorescence on reprogramming day 5 with the following antibodies: mouse α phospho-histone H2A.X-Ser139 (Millipore #05-636), rabbit α phospho-RPA2Ser33 (Invitrogen #PA5-39809), rabbit α 53BP1 H-300 (Santa Cruz #22760, 1:50 dilution). Quality controls: the rabbit α -phospho-RPA2Ser33 does not react to S33A mutant.⁷¹ The antibody α phospho-histone H2A.X-Ser139 does not react to S139A-mutant H2AX.⁶⁷ 53BP1 foci co-localized with γ H2AX (Figure S4G).

The numbers of phospho-H2AX(S139) and phospho-RPA(S33) foci were counted in an automated manner by scanning stained slides with the Metafer4-Metacyte system and applying the same counting algorithm to all samples. Only large, unmistakable foci were considered and small specs of staining were excluded to avoid false positives. 53BP1 foci were counted with the Olympus cellSens software. For detection of Rad51, iPSC lines were irradiated with 10Gy and stained with Rad51 (Ab-1) rabbit pAb (Millipore #PC130) 1.5h post IR. Quality control: this antibody has previously been shown to detect ATR dependent Rad51 foci formation.⁷² Foci numbers were determined by using the counting and analysis function of the Olympus cellSens software. Nanog expression was evaluated on reprogramming day 20 with rabbit α Nanog (Reprocell #RCAB001P2P) antibody. TRA-1-60 was detected in human cells with Alexa Fluor 488 conjugated mouse α human TRA-1-60 (BD Biosciences #BD560173).

DNA fiber analysis

DNA fiber analysis on *Brca1*, *Smarca1* and *53bp1* combination mutants during reprogramming was carried out as described in Terret et al.⁷³ Briefly, fibroblasts of different genotypes were incubated on reprogramming day 5 with 25 μ M CldU for 30min, washed 3 times with warm PBS and incubated with 125 μ M IdU for another 30min. Fork stalling was induced by a 5h-long treatment with 2mM hydroxyurea (HU). In an alternative fiber assay, fork stalling was induced by treatment with 2 μ M pyridostatin (PDS) during the 30min incubation with 125 μ M IdU.

Fiber experiments with the ABC genotype collection and the *Brca1*^{tr/+} genotype were performed on uninfected immortalized MEFs. Cells from the ABC genotypes were incubated with 200 μ M IdU for 20min, washed three times with PBS and then incubated with 100 μ M CldU for 20min. Fork stalling was induced by treatment with 2mM HU for 1.5h. In some conditions, 50 μ M mirin was added during the pulse labelling steps with IdU and CldU as well as during incubation with HU. Immortalized MEFs from the *Brca1*^{tr/+} genotype and controls were incubated with 50 μ M CldU for 20min, followed by 3 washes with PBS and 250 μ M IdU for 20min. Fork stalling was induced by treatment with 2mM HU for 1.5h.

Fibers were stretched on slides and stained with BrdU/CldU (Biorad # OBT0030) and BrdU/IdU (BD # 347580) antibodies. Imaging was performed with a 100x objective on an Olympus microscope and fiber length was measured with Olympus cellSens imaging and analysis software.

HDR assay

The HDR competence of the different genotypes was evaluated in mouse induced pluripotent stem cells (iPSCs) with a CRISPR-Cas9-based assay where a zsGreen repair template is targeted to the Hsp90 genomic locus. This strategy has been described in detail by Mateos-Gomez et al.³² In short, 200-300x10³ exponentially growing iPSCs were transfected with 200ng Cas9-puromycin vector and 800ng zsGreen repair template with Jetprime transfection reagent (VWR #89129-922) as outlined in the manufacturer's instructions. Media was changed ~20h post transfection for 24h. To enrich for Cas9-transfected cells, the plates were treated with 1 μ g/ml puromycin (Thermo Fisher #A11138-03) for ~20h. Flow cytometry for zsGreen was performed on the 3rd day of recovery from puromycin selection. To exclude potentially non-transfected cells, the efficiency of single versus dual allele targeting was compared.

Proliferation and apoptosis

To evaluate proliferation, infected fibroblasts on reprogramming day 2 were incubated with 5 μ M Cell Trace CFSE proliferation dye (Thermo Fisher # C34554) for 20min at 37°C as outlined in the manufacturer's protocol. Cells were then changed to fresh mouse ES cell media, composed of Knockout DMEM (Life Technologies #10829-018), 15% Knockout Serum Replacement (Life Technologies #10828-028), Glutamax (Thermo Fisher Scientific #35050079), MEM NEAA (Life Technologies #11140050), PenStrep (Thermo Fisher Scientific 15140163), 2-mercaptoethanol (Life Technologies #21985-023) and 10ng/ μ l LIF (eBioscience #34-8521-82), supplemented with 1 μ g/ml doxycycline (Sigma # D9891). Three days post incubation with CFSE (reprogramming day 5) cells were harvested for flow cytometry.

For apoptosis analysis, cells were collected on reprogramming day 5 and stained without fixation with the Annexin V-FITC apoptosis detection kit (Sigma # APOAF-20TST) according to protocols provided by the manufacturer. The numbers of early and late apoptotic cells were determined by flow cytometry for Annexin V-FITC and propidium iodide (PI). Early apoptosis is marked by Annexin V staining only, while late apoptotic cells stain for both Annexin V and PI.

Nanog detection

Cells were harvested on reprogramming day 20 and fixed in 4% paraformaldehyde for 15 min at RT. Staining was performed by standard protocol with rabbit α Nanog primary AB (Reprocell #RCAB001P2P) for 1h at RT, followed by 3 washes with 3% BSA in

PBST (PBS + 0.1% Triton) and a secondary Alexa Fluor 488 donkey anti-rabbit IgG (H+L) (Thermo Fisher #A21206) for another hour at RT. The cell suspension was then filtered through a BD Falcon 12 × 75-mm tube with a cell strainer cap (BD Falcon #352235) and analyzed on a BD Fortessa flow cytometer. Data was plotted with FlowJo v.10 and the positive gate was set according to a secondary antibody only negative control.

S1 nuclease assay

Exponentially growing cells on reprogramming day 10 or established iPSC lines were pulse-labeled with 30 μ M IdU for 15 min, washed with PBS twice, and exposed to 150 μ M CldU for 45 min. After exposure to the second nucleotide analog, cells were collected, washed in 1x PBS and permeabilized with CSK buffer (100mM NaCl, 10mM MOPS pH7, 3mM MgCl₂, 300mM sucrose and 0.05% Triton X-100 in water) for 10 min on ice and centrifuged at \sim 4,600g for 5 min at 4°C. Permeabilized cells were then treated with 100 μ l of S1 buffer (30mM sodium acetate pH4.6, 10mM zinc acetate, 5% glycerol, 50mM NaCl in water) with or without the S1 nuclease (Thermo Fisher Scientific #18001-016) at 10U/ml for 15 min at 37°C. Cells were pelleted at \sim 4,600g for 5 min at 4°C and then resuspended in PBS. Labeled cells were harvested and resuspended in PBS at a concentration of 2×10^5 cells/ml. Two microliters of cell suspension were spotted onto a pre-cleaned glass slide and lysed with 10 μ l of spreading buffer (0.5% SDS in 200mM Tris-HCl, pH7.4 and 50mM EDTA). After 6min, the slides were tilted at 15° relative to a horizontal surface, allowing the DNA fibers to spread. Slides were air-dried, fixed in methanol and acetic acid (3:1) for 2 min, rehydrated in PBS for 10 min and denatured with 2.5M HCl for 50 min at room temperature. Slides were then rinsed in PBS and blocked in PBS + 0.1% Triton X-100 (PBST) + 5% BSA for 1h at RT. Rat anti-BrdU (1:100, Abcam #ab6326) and mouse anti-BrdU (1:100, Becton Dickinson #347580) were then applied to detect CldU and IdU, respectively. After a 1h incubation, slides were washed in PBS and stained with Alexa Fluor 488-labeled goat anti-mouse IgG1 antibody and Alexa Fluor 594-labeled goat anti-rat antibody (1:300 each, Thermo Fisher Scientific). Slides were mounted in Prolong Gold Antifade (Thermo Fisher Scientific #P10144) and stored at -20° C. Replication tracks were imaged on a Nikon Eclipse 90i microscope, fitted with a PL Apo 40X/0.95 numerical aperture (NA) objective. The length of each track was determined manually using the segmented line tool on ImageJ software (NIH). The pixel values were converted into μ m using the scale bar generated by the microscope software. Size distribution of track lengths from individual DNA fibers was plotted as scatter dot plot with a line representing the median.

QUANTIFICATION AND STATISTICAL ANALYSIS

Each genotype in an experiment was present in at least 3 biological replicates (MEFs from different embryos of the same genotype). Samples with only two biological replicates were not used for statistical analysis or to solely base conclusions on, and are instead shown as affirming results with other genotypes.

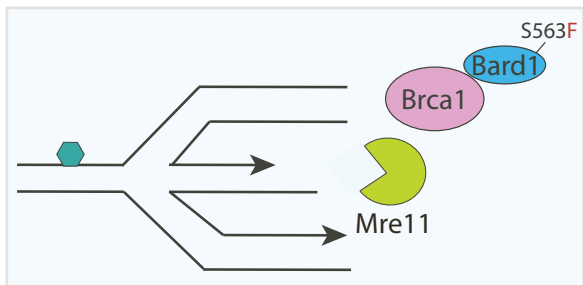
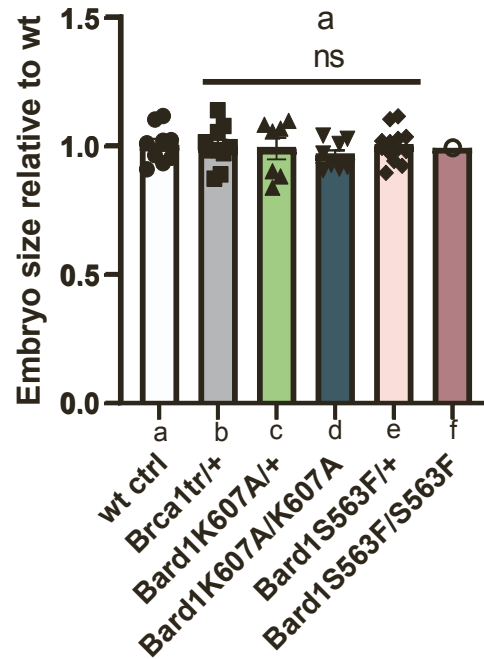
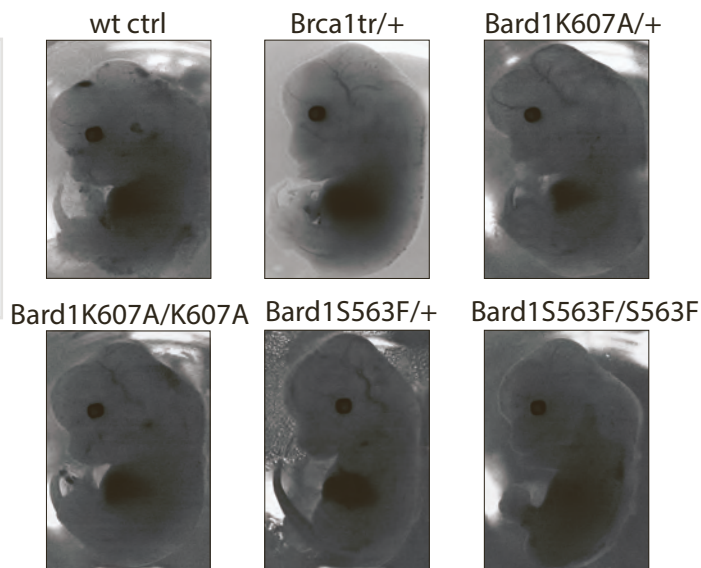
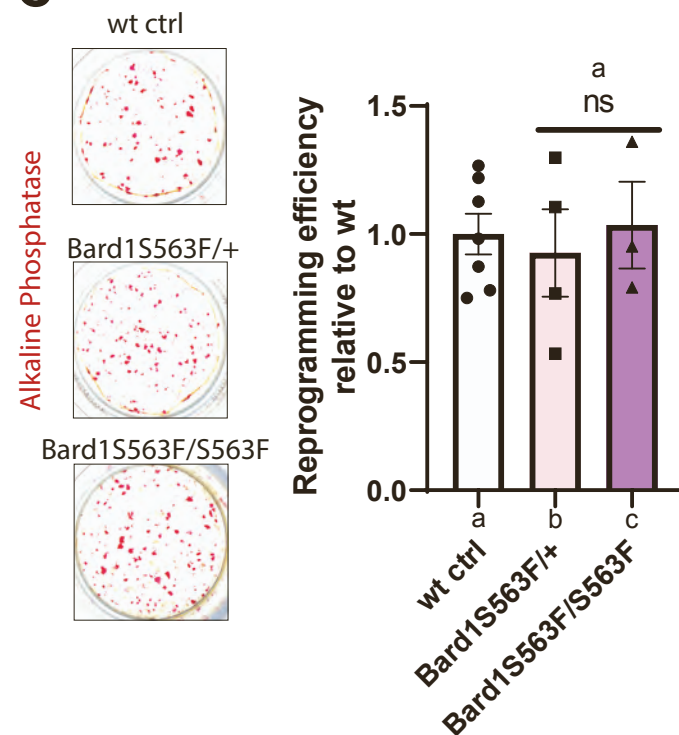
Statistical calculations were carried out with GraphPad Prism. Comparisons between multiple experimental groups or genotypes were performed with one-way ANOVA and analyzed with Sidak's multiple comparisons test. For all ANOVA analyses, CI = 95%. In the cases where only two experimental groups were available, statistical significance was evaluated with a two-tailed, unpaired Student's t test. Statistically significant differences in DNA fiber track length distributions in the S1 nuclease assay were determined by a Mann-Whitney test. * $p < 0.05$, ** $p < 0.01$ and *** $p < 0.001$ and **** $p < 0.0001$. All error bars represent the standard error of the mean (SEM). Figures were prepared with Adobe Illustrator, the Graphical Abstract was made with BioRender.

Cell Reports, Volume 43

Supplemental information

**BRCA1 and 53BP1 regulate reprogramming efficiency
by mediating DNA repair pathway choice
at replication-associated double-strand breaks**

Daniela Georgieva, Ning Wang, Angelo Tagliatela, Stepan Jerabek, Colleen R. Reczek, Pei Xin Lim, Julie Sung, Qian Du, Michiko Horiguchi, Maria Jasin, Alberto Ciccia, Richard Baer, and Dieter Egli

A**B****C**

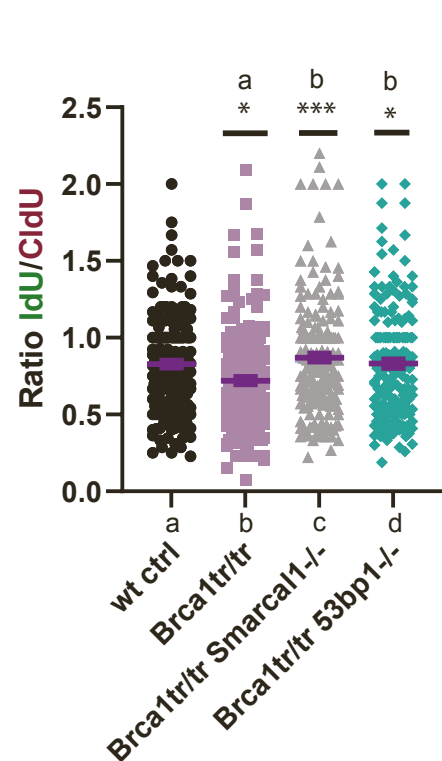
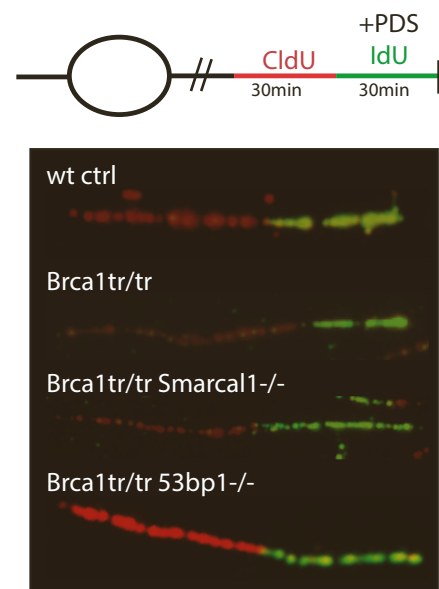
Supplementary Figure 1. Role of Bard1 mediated stalled replication fork stability in reprogramming.

A). Schematic illustrating the role of Bard1S563 in stalled fork protection (SFP). The Bard1S563F point mutation prevents the recruitment of the Brca1/Bard1 heterodimer to reversed stalled replication forks, which makes them vulnerable to Mre11-dependent degradation. **B**). Morphology of E13.5 embryos and quantification of size. Statistical significance was evaluated by one-way ANOVA.; wt ctrl n = 9, Brca1tr/+ n = 10, Bard1K607A/+ n = 7, Bard1K607A/K607A n = 8, Bard1S563F/+ n = 13, Bard1S563F/S563F n = 1.

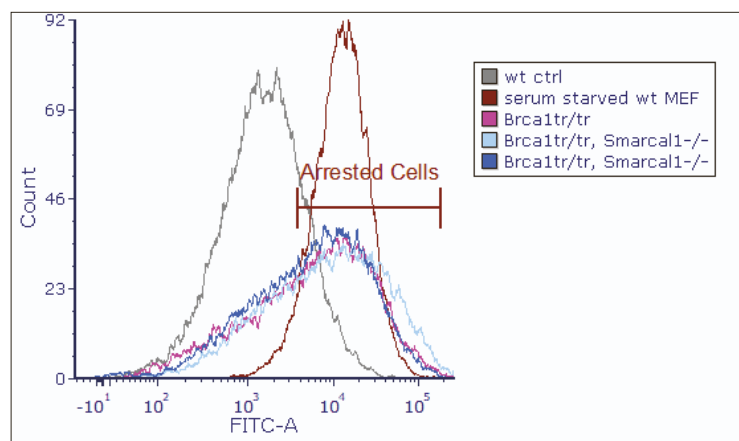
C). Alkaline phosphatase (AP) staining on reprogramming day 20 and reprogramming efficiency quantification. Data was analyzed by one-way ANOVA.; wt ctrl n = 7, Bard1S563F/+ n = 4, Bard1S563F/S563F n = 3.

Supplementary Figure 2

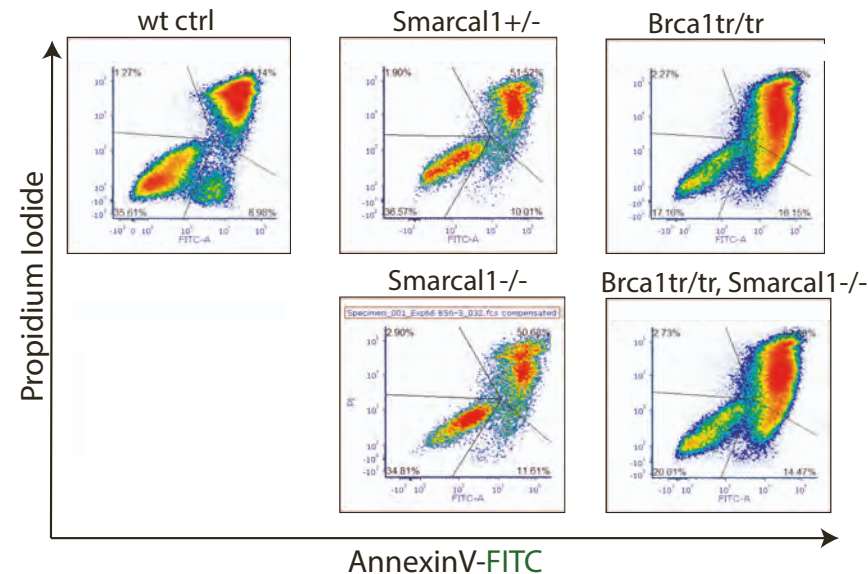
A



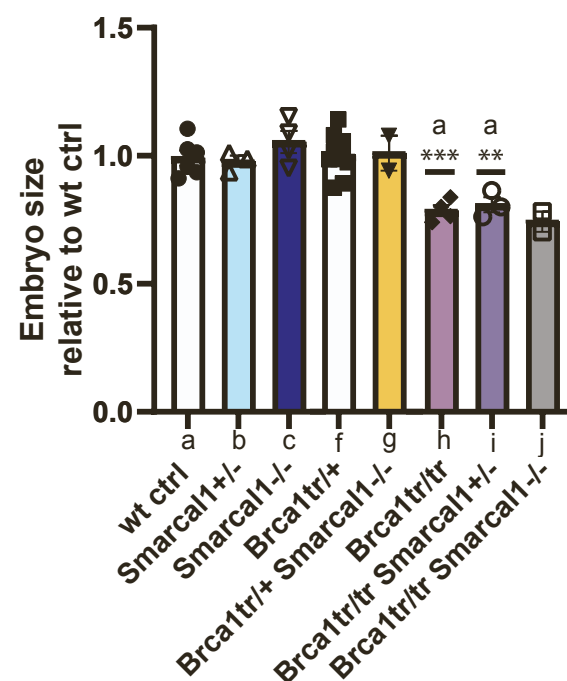
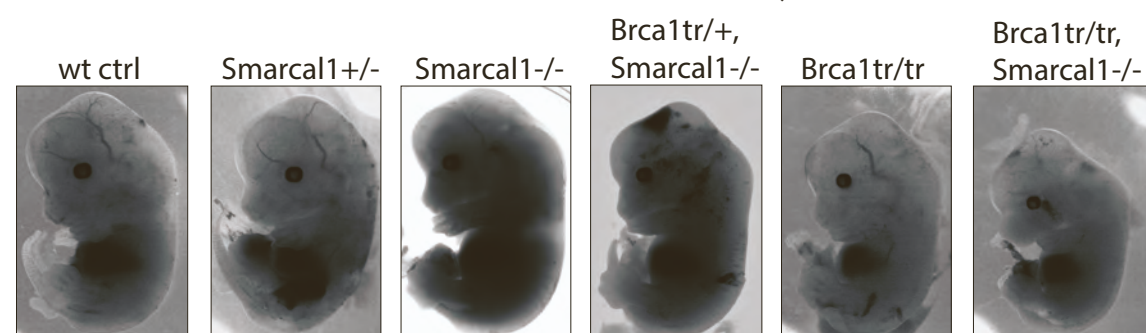
B



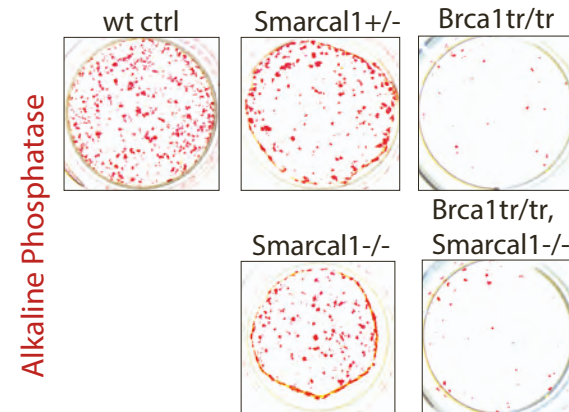
C



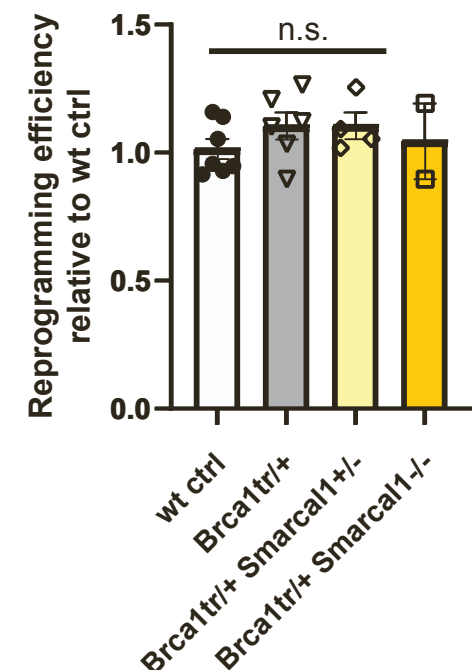
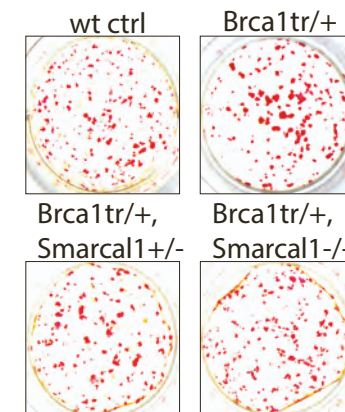
D



E

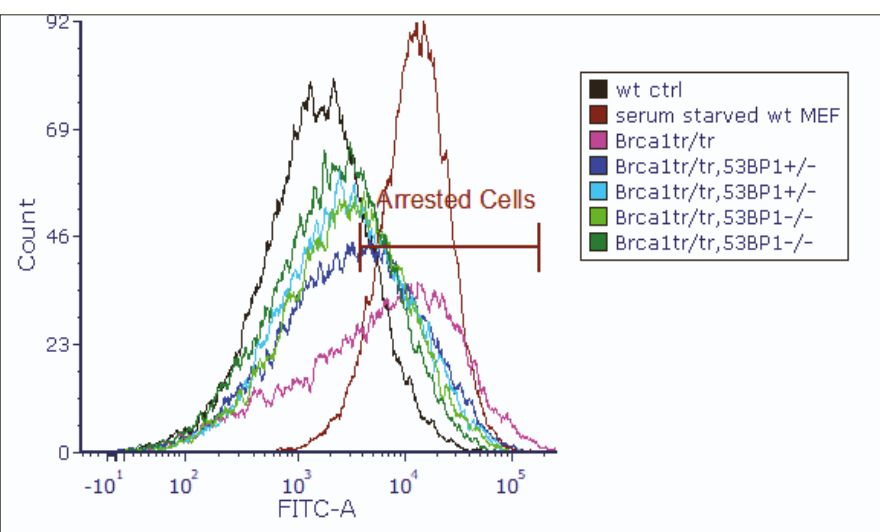
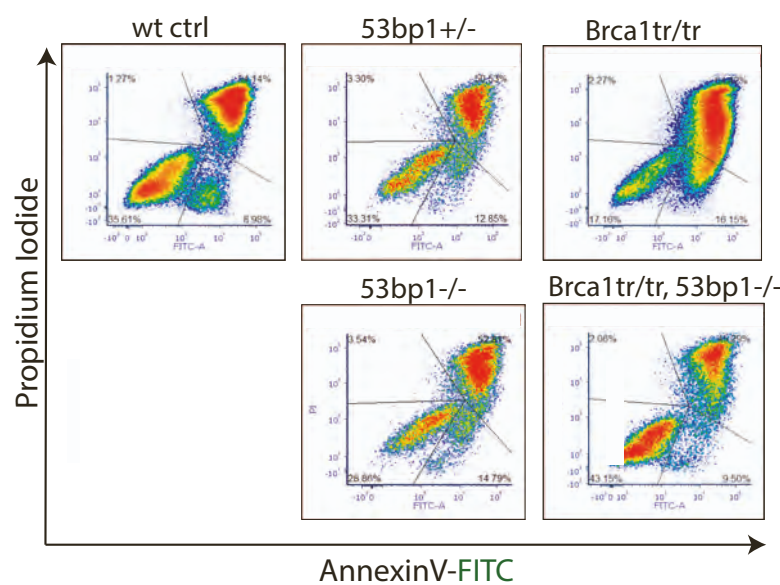
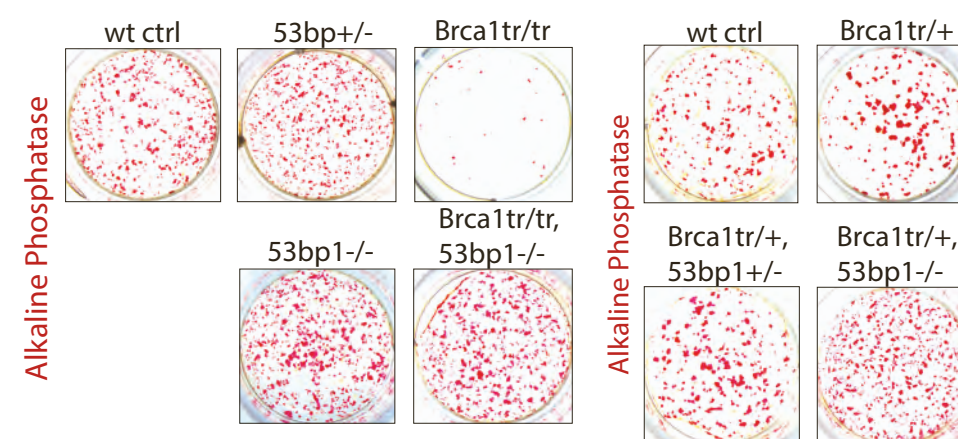
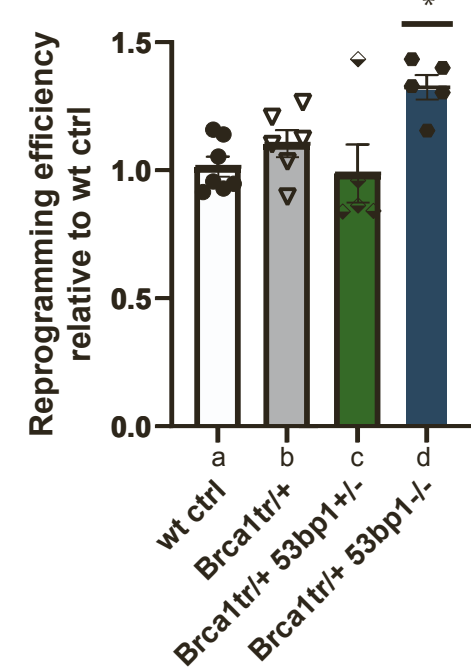
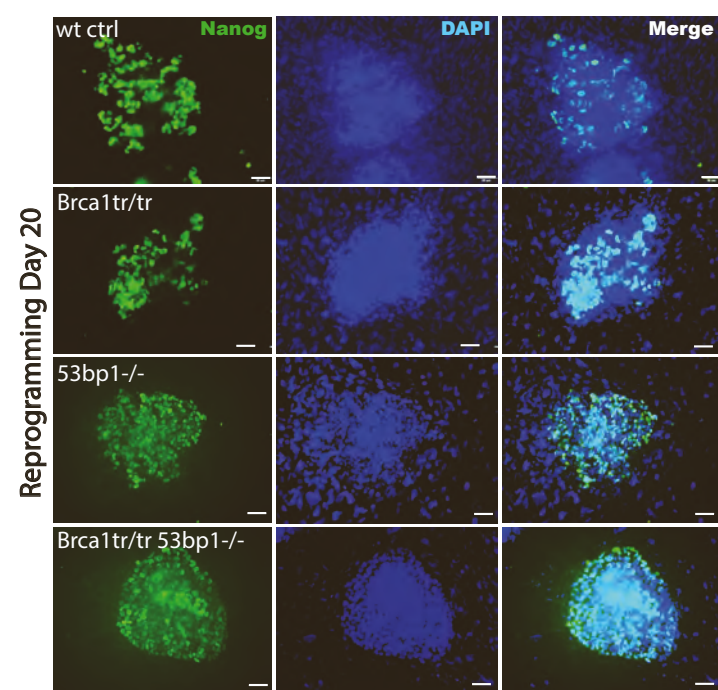
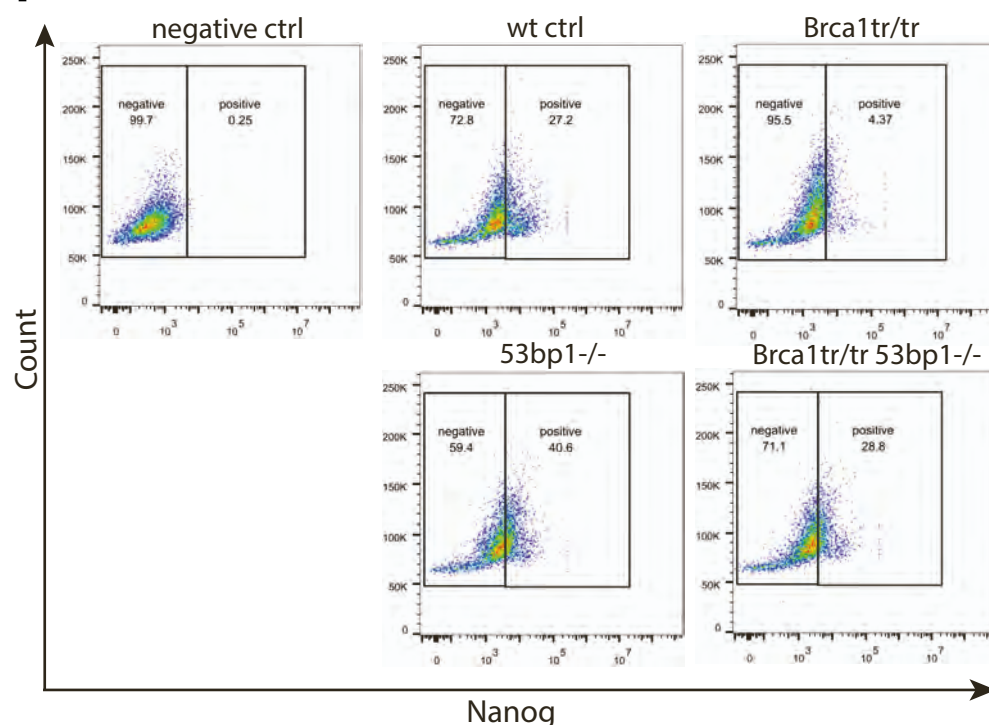
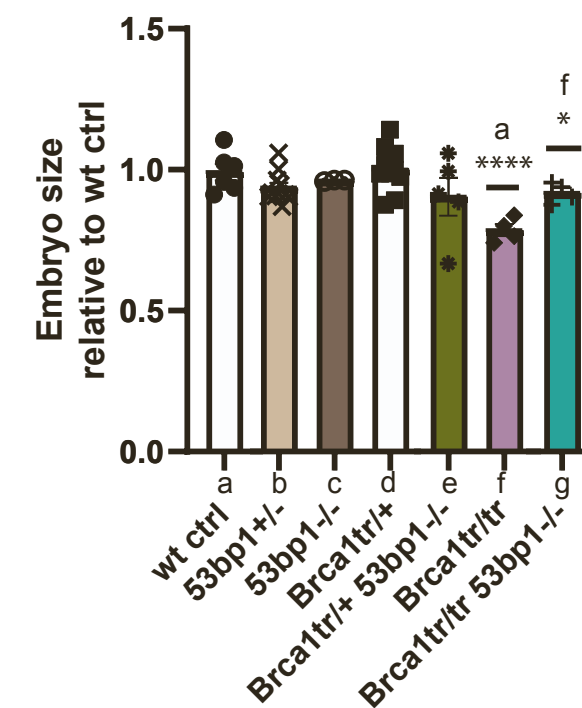
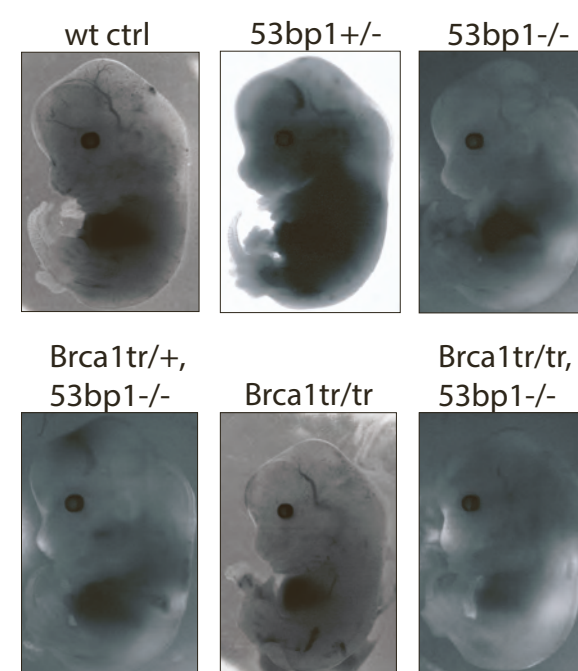
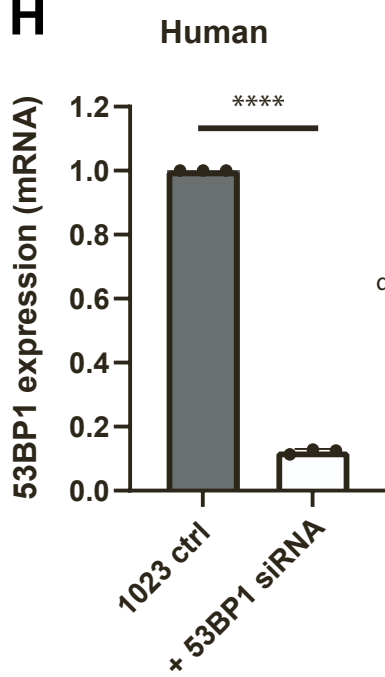
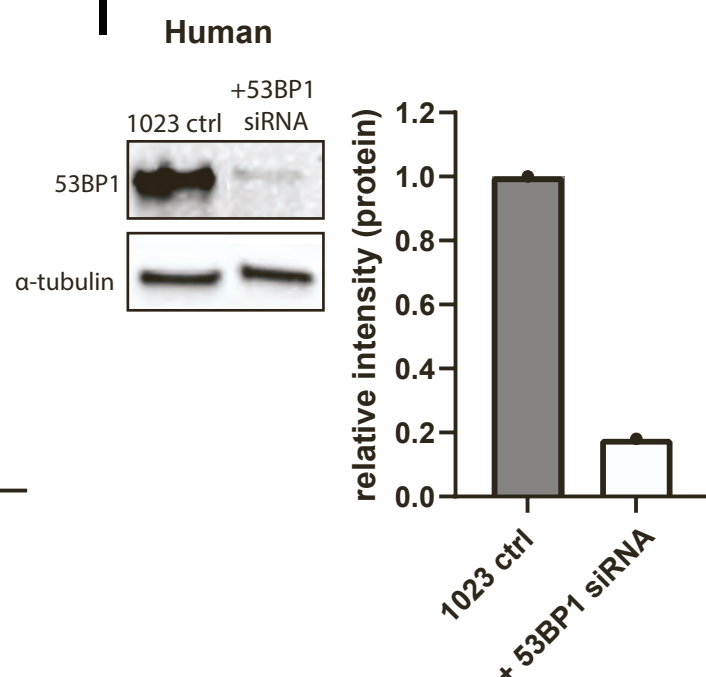
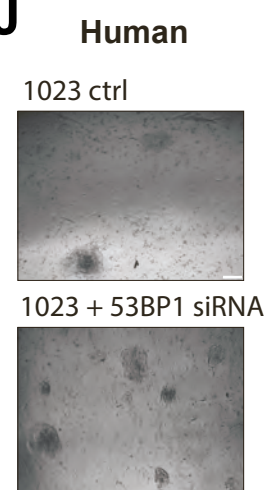
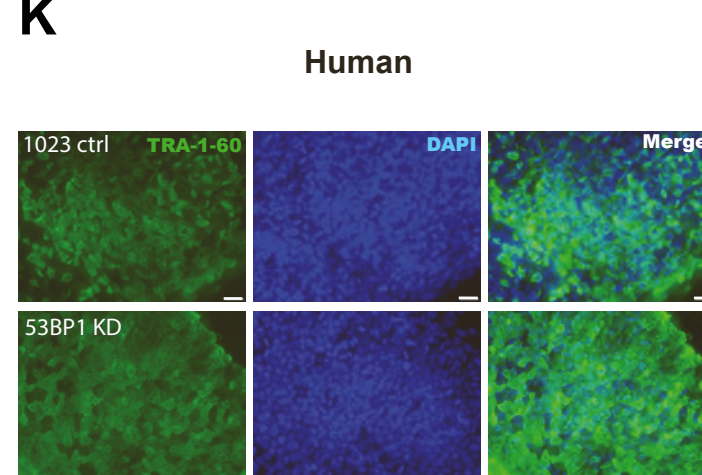
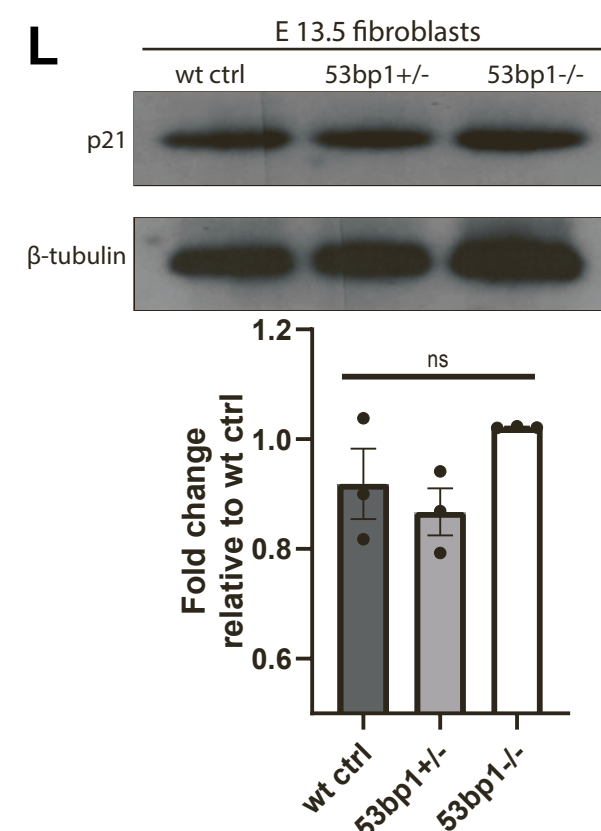
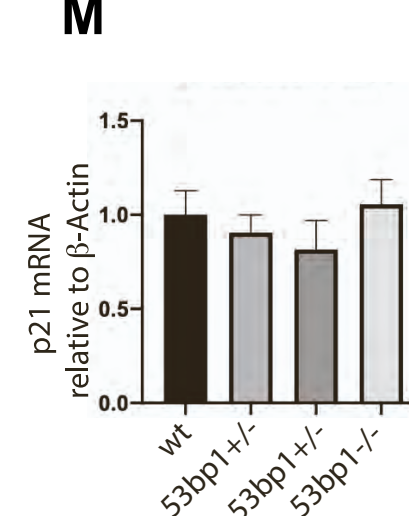


F



Supplementary Figure 2. Smarcal1 is not required for somatic cell reprogramming and restoring stalled fork stability does not improve reprogramming in Brca1 mutant cells.

A). DNA fiber analysis in a fork stalling assay on reprogramming day 5 with pyridostatin (PDS). Data was collected from >180 fibers per genotype and analyzed by one-way ANOVA. B). Flow cytometry plots of CFSE cytoplasmic dye retention on reprogramming day 5. Serum starved cells exhibit a bright peak, centered around 104, while cycling cells dilute the dye and the peak moves to the left. C). Flow cytometry for Annexin V-FITC and propidium iodide (PI) on reprogramming day 5. Early apoptotic cells stain for Annexin V only, while late apoptosis is marked by double staining for Annexin V and PI due to an increase in membrane permeability. D). Morphology and quantification of E13.5 embryo size. Statistical analysis was performed with one-way ANOVA.; wt ctrl n = 6, Smarcal1+/- n = 3, Smarcal1-/- n = 4, Brca1tr/+ n = 10, Brca1tr/+Smarcal1-/- n = 2, Brca1tr/tr n = 4, Brca1tr/trSmarcal1+/- n = 3, Brca1tr/trSmarcal1-/- n = 2. E). Extended Alkaline phosphatase (AP) staining panel. F). AP staining and reprogramming efficiency quantification of Brca1 heterozygous cells with different Smarcal1 genotypes. Control and samples are from mates of the same litter. wt ctrl n = 7, Brca1tr/+ n = 6, Brca1tr/+ Smarcal1+/- n = 4, Brca1tr/+Smarcal1-/- n = 2. ***p<0.001, **p<0.01

A**B****C****D****E****F****G****H****I****J****K****L****M**

Supplementary Figure 3. Role of 53BP1 in somatic cell reprogramming.

A). Flow cytometry plots of CFSE cytoplasmic dye retention on reprogramming day 5. Serum starved cells exhibit a bright peak, centered around 10^4 , while cycling cells dilute the dye and the peak moves to the left. **B).** Flow cytometry for Annexin V-FITC and propidium iodide (PI) on reprogramming day 5. Early apoptotic cells stain for Annexin V only, while late apoptosis is marked by double staining for Annexin V and PI due to an increase in membrane permeability. **C).** Extended Alkaline phosphatase (AP) staining panel for indicated genotypes with matched wild type cells from sibling littermates. **D).** Reprogramming efficiency quantification. The comparison between Brca1tr/+ and Brca1tr/+53bp1-/- was performed with a two-tailed, unpaired student's t-test.; wt ctrl n = 7, Brca1tr/+ n = 6, Brca1tr/+53bp1+/- n = 5, Brca1tr/+53bp1-/- = 5. **E).** Immunofluorescence staining for pluripotency marker Nanog Scale bar: 5 μ m. .

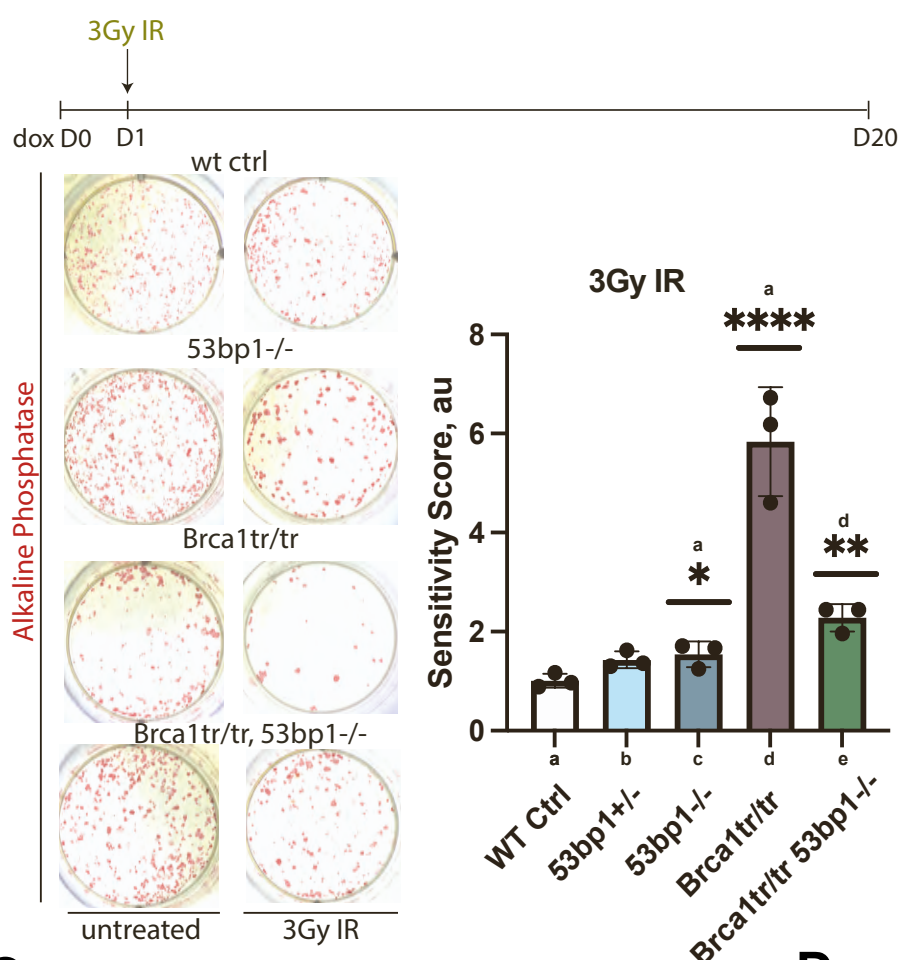
F) Flow cytometry plots showing the percentage of Nanog positive cells in the indicated genotypes on reprogramming Day 20.

G). Morphology and quantification of E13.5 embryo size. Statistical analysis was performed with one-way ANOVA.

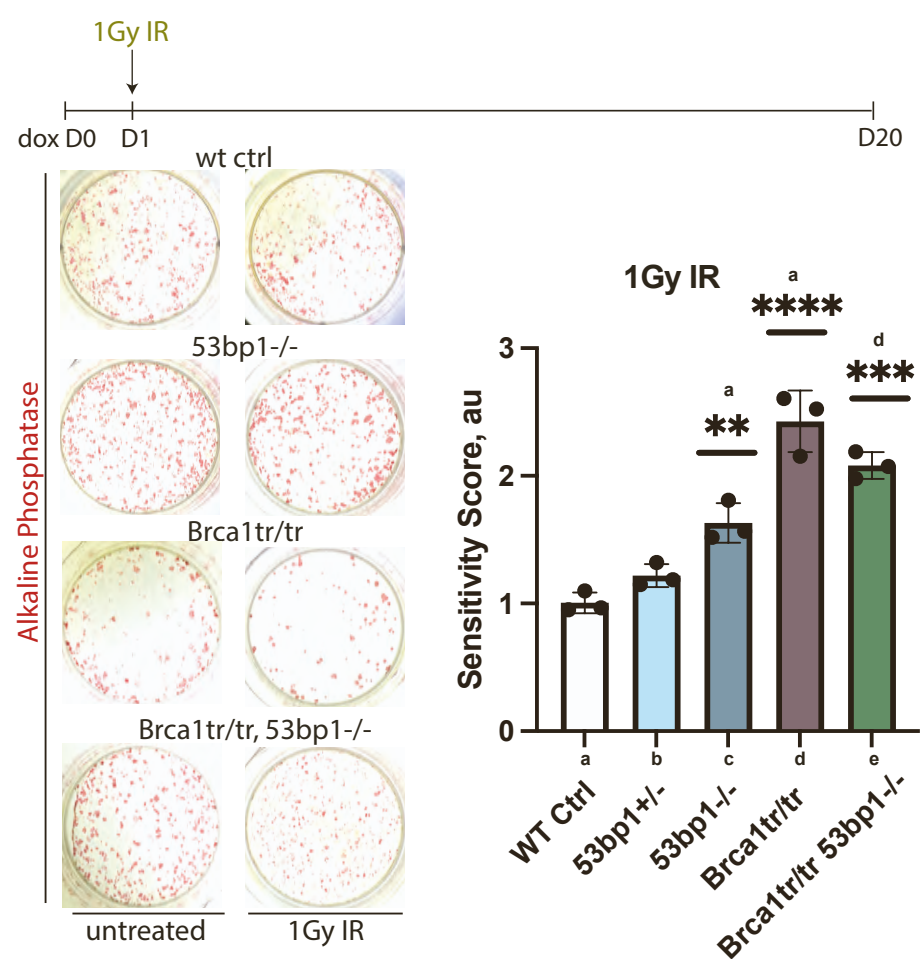
wt ctrl n = 6, 53bp1+/- n = 11, 53bp1-/- n = 3, Brca1tr/+ n = 10, Brca1tr/+53bp1-/- n = 5, Brca1tr/tr n = 4, Brca1tr/tr53bp1-/- n = 4. **H).** qPCR for 53BP1 expression 2 days after siRNA transfection. Data was analyzed with an unpaired, two-tailed student's t-test.; n = 3 for each genotype. **I).** WB and quantification of 53BP1 protein levels 2 days post siRNA transfection. **J).** Bright field images of human iPS cell colonies on day 20 post transduction of 1023 adult skin biopsy fibroblasts with the reprogramming factors.; scale bar = 200 μ m. **K).** Immunofluorescence for human pluripotent stem cell marker TRA-1-60 of a representative iPS colony on day 25 post transduction with the reprogramming factors.; scale bar = 50 μ m. **L).** Western blot and signal quantification for p21 protein in E13.5 mouse fibroblasts of the indicated genotypes. Data from was analyzed by one-way ANOVA; n = 3 for each genotype. **M).** RT-qPCR for mRNA levels in E13.5 mouse fibroblasts of the indicated genotypes. Wt was normalized to 1.

Supplementary Figure 4

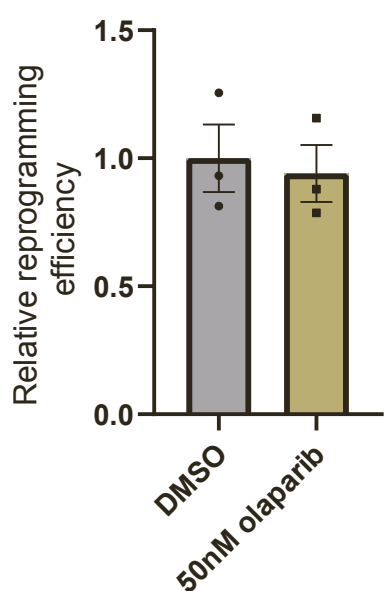
A



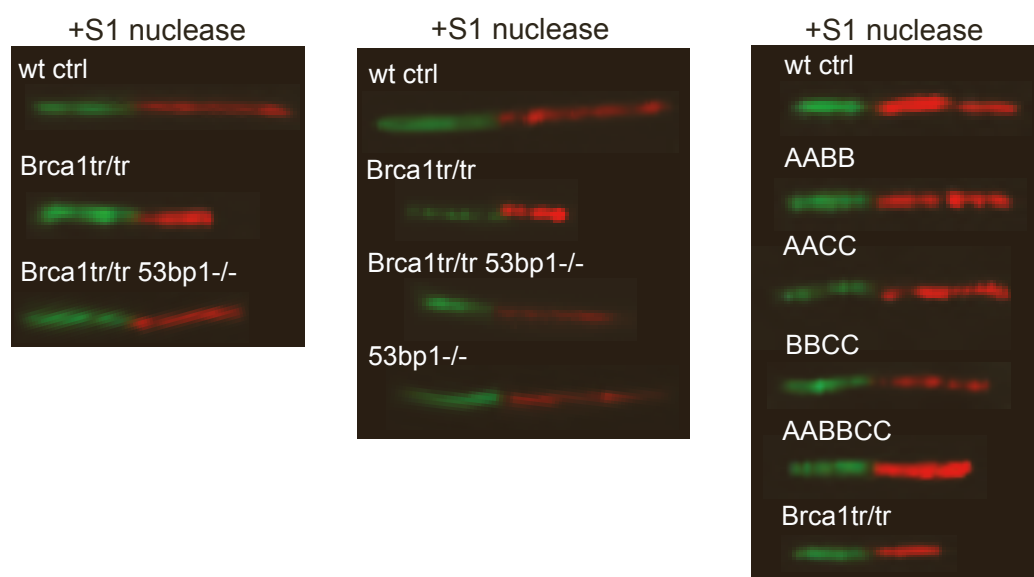
B



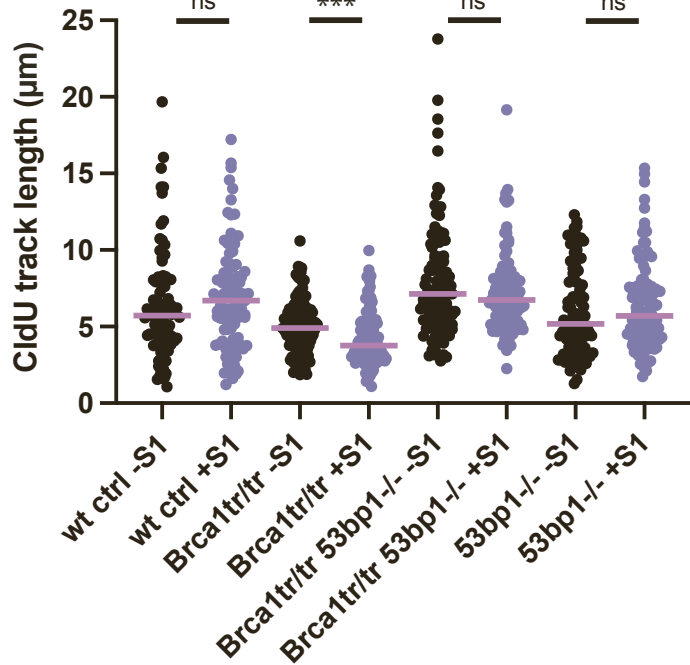
C



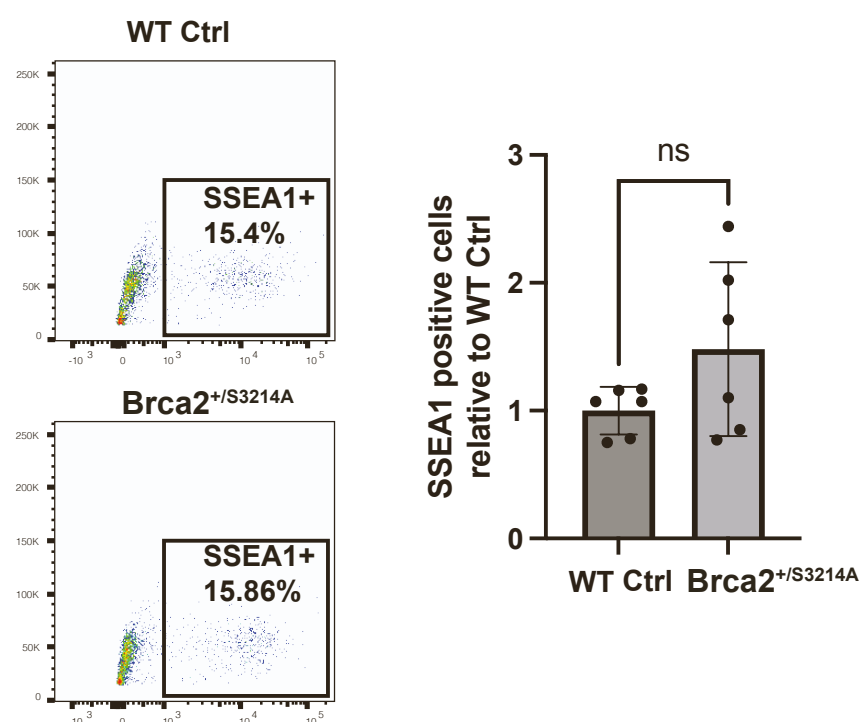
D



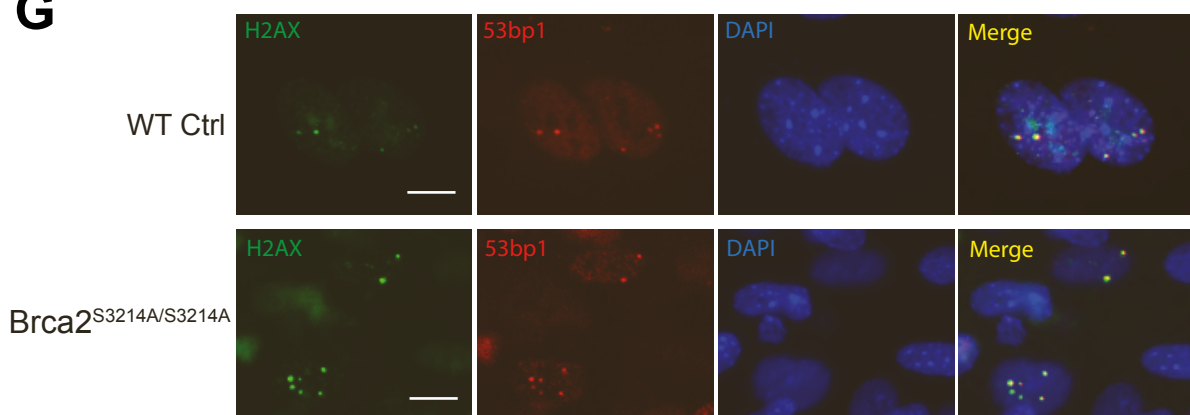
E



F



G



Supplementary Figure 4. Replication gap suppression is dispensable for reprogramming

A-B). AP staining and genotype-specific sensitivity evaluation to treatment with a single dose of 3Gy IR (A) or 1Gy IR (B) 1 day post reprogramming factor induction. Data was analyzed by one-way ANOVA, except for the comparison between wt ctrl and Brca1tr/tr 53bp1-/-, which was carried out with an unpaired two-tailed student's t-test; n = 3 for each genotype. **C).** Reprogramming efficiency quantification of wild type cells after olaparib treatment. **D).** Representative images of DNA fibers from iPS cell lines of the indicated genotypes, treated with S1 nuclease. Wild type fibers are from an experiment performed in parallel. **E).** Dot plot of CldU track length in cells of the indicated genotypes, harvested on reprogramming day 10; ≥ 90 fibers were measured per experimental condition and statistical significance was determined with a two-tailed Mann-Whitney test; the purple line marks the median. **F).** Flow cytometry plots showing the percentage of SSEA1 positive cells in the indicated genotypes on Day 12; n=6. The statistical analysis was performed with an unpaired, two-tailed student's t-test. **G).** Immunofluorescence DSB markers phospho H2AX (S139) and 53bp1 on reprogramming day 5 in WT ctrl and Brca2^{S3214A/S3214A} fibroblasts. Scale bar: 5μm.

Genotype	Phenotype	γ H2AX foci	RPA(S33) foci	53bp1 foci	Apoptosis	Reprogramming Efficiency	Cancer Susceptibility	Embryo Size
<i>Bard1</i> ^{K607A/+}	HDR+ SFP-					same as wt	No	same as wt
<i>Bard1</i> ^{K607A/K607A}	HDR+ SFP-	same as wt	same as wt	same as wt		same as wt	No	same as wt
<i>Bard1</i> ^{S563F/+}	HDR+ SFP-					same as wt	No	same as wt
<i>Bard1</i> ^{S563F/S563F}	HDR+ SFP-			same as wt		same as wt	No	same as wt
<i>Brca1</i> ^{tr/+}	HDR+ SFP-	same as wt	same as wt	same as wt		same as wt	No	same as wt
<i>Smarcal1</i> ^{+/-}	HDR+ SFP+				same as wt	same as wt		same as wt
<i>Smarcal1</i> ^{-/-}	HDR+ SFP+				same as wt	same as wt		same as wt
<i>Brca1</i> ^{tr/+} <i>Smarcal1</i> ^{+/-}	HDR+ SFP- *					same as wt		same as wt
<i>Brca1</i> ^{tr/+} <i>Smarcal1</i> ^{-/-}	HDR+ SFP+					same as wt		same as wt
<i>Brca1</i> ^{tr/tr}	HDR- SFP-	↑↑↑	↑↑↑	↑↑↑	↑↑↑	↓↓↓	Yes	↓
<i>Brca1</i> ^{tr/tr} <i>Smarcal1</i> ^{+/-}	HDR- SFP- *					↓↓↓		↓
<i>Brca1</i> ^{tr/tr} <i>Smarcal1</i> ^{-/-}	HDR- SFP+	same as wt	↑	↑↑↑	↑↑↑	↓↓↓		↓
<i>53bp1</i> ^{+/-}	HDR+ SFP+				same as wt	same as wt		same as wt
<i>53bp1</i> ^{-/-}	HDR++ SFP+/-				same as wt	↑	Yes	same as wt
<i>Brca1</i> ^{tr/+} <i>53bp1</i> ^{-/-}	HDR++ SFP+/- *					↑		same as wt
<i>Brca1</i> ^{tr/tr} <i>53bp1</i> ^{-/-}	HDR+ SFP+/- †	same as wt	same as wt	none	same as wt	same as wt	No	same as wt
<i>AABB</i>	HDR+ SFP+	same as wt				same as wt	No	same as wt
<i>BBCC</i>	HDR(-) SFP+, RGS+	same as wt				↓	nd	same as wt
<i>AACC</i>	HDR(-) SFP+, RGS+	same as wt				↓	nd	same as wt
<i>AABBCC</i>	HDR- SFP-	↑				↓↓↓	nd	↓
<i>Brca2</i> ^{S3214A/S3214A}	HDR+SFP-RGS-	nd	nd	nd	nd	same as wt		
<i>Brca2</i> ^{Δ27/Δ27}	HDR-SFP-RGS-	nd	nd	nd	nd	↓↓↓		
<i>Brca2</i> ^{Δ27/+}	HDR+SFP-RGS-	nd	nd	nd	nd	same as wt		

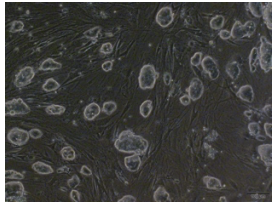
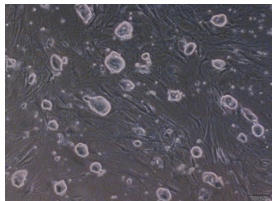
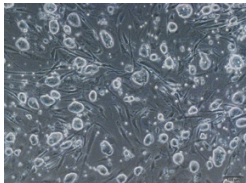
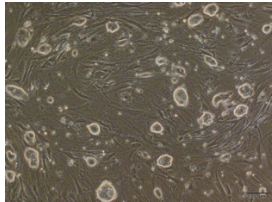
Supplementary Table 1. Reprogramming genotype collection. Molecular characteristics, reprogramming efficiency and tumor susceptibility is indicated for each genotype-phenotype pair. Phenotypic deficiencies are colored in magenta; each symbol refers only to the abbreviation that immediately precedes it. HDR = homology directed repair; SFP = stalled fork protection; RGS = replication gap suppression.

* SFP phenotype inferred from other genotypes

† improved, but not completely rescued

+/- for 53bp1 genotypes is based on the biological variability of the effect of 53BP1 on replication fork stability (Liu et al., 2020).

Nd = not determined

Genotype	Photo (if available)	Genotype	Photo (if available)
Wt		<i>Brca1tr/+</i> , <i>53bp1-/-</i>	na
<i>Brca1 tr/+</i>		<i>Brca1tr/tr</i> , <i>53bp1+/-</i>	na
<i>Brca1 tr/tr</i>		<i>Brca1tr/tr</i> , <i>53bp1-/-</i>	na
<i>Smarcal1 +/-</i>		<i>AABB</i>	na
<i>Smarcal1 -/-</i>		<i>BBCC</i>	na
<i>Brca1tr/+</i> , <i>Smarcal1+/-</i>		<i>AACC</i>	na
<i>Brca1tr/+</i> , <i>Smarcal1-/-</i>		<i>AABBCC</i>	
<i>Brca1tr/tr</i> , <i>Smarcal1+/-</i>		<i>Brca2 SA/+ iPSC</i>	na
<i>Brca1tr/tr</i> , <i>Smarcal1-/-</i>		<i>Brca2 SA/SA iPSC</i>	na
<i>53bp1+/-</i>			na
<i>53BP1-/-</i>			na
<i>Brca1tr/+</i> , <i>53bp1+/-</i>			na

Supplementary Table 2 | Genotypes of iPS cell lines and associated images. Na: not applicable; no images were taken, cell lines were phenotypically normal.

Bard1 ^{S563F/+} Bard1 ^{S563F/S563F}	GCAGGTGCTCTACCCTC AAC	AACCTGGCCATCAACAT G
Bard1 ^{K607A/+} Bard1 ^{K607A/K607A}	CACGTGGTTGCTGGAA ATTG	ATGTAAAGGAGCCAGC AGC
Brcal ^{tr/+} Brcal ^{tr/tr}	TGCTCACTCTGTGCCCT CAA	TCCATTCTCCCCGCTTCT GT
Smarcal1 ^{+/-} Smarcal1 ^{-/-}	CCGCTCTAACCTGGGA ACAC	GTGACAGACAACAGCC AGCC TCGTGGTATCGTTATGC GCC
53bp1 ^{+/+}	AGGAGACTGAAGAACC AATCG	CTCAGTTTTCTGGGCC TCCT
53bp1 ^{+/-} 53bp1 ^{-/-}	GTCAGGGTTTCACTGG CTTG	CCTTCTTGACGAGTTCTT
Abraxas ^{S404A/+} Abraxas ^{S404A/S404A}	CAGCAGGCACCAAGAC AAGG	TCTGTGTATTAATCCGA GAGGCAAAGA
Bach1 ^{S994A/+} Bach1 ^{S994A/S994A}	GCCAAGTGTCCCAGCT CAAA	TCAGTGTCCCAGGCAAC TAAG
Ctip ^{S326A/+} Ctip ^{S326A/S326A}	TAGCAAAAGTCCTCAG TGGGC	TGTTGCTAAAGGGAGCT GTC

Supplementary Table 3. Sequences of genotyping primers. For each genotype, forward and reverse primer pairs are provided.